Far field splitting by iteratively reweighted ℓ^1 minimization

Roland Griesmaier* and John Sylvester†

June 29, 2015

Abstract

The aim of far field splitting for time-harmonic acoustic or electromagnetic waves is to decompose the far field of a wave radiated by an ensemble of several compactly supported sources into the individual far field components radiated by each of these sources separately. Without further assumptions this is an ill-posed inverse problem. Observing that far fields radiated by compactly supported sources have nearly sparse representations with respect to certain suitably transformed Fourier bases that depend on the approximate source locations, we develop an ℓ^1 characterization of these far fields and use it to reformulate the far field splitting problem as a weighted ℓ^1 minimization problem in the spirit of basis pursuit. To this end we assume that some a priori information on the locations of the individual source components is available. We prove that the unique solution to the weighted ℓ^1 minimization problem coincides with the solution to the far field splitting problem, and we discuss its numerical approximation. Furthermore, we propose an iterative strategy to successively improve the required a priori information by solving a sequence of these weighted ℓ^1 minimization problems, where estimates of the approximate locations of the individual source components that are used as a priori information for the next iteration are computed from the value of the current solution. This also gradually decreases the ill-posedness of the splitting problem, and it significantly improves the quality of the reconstructions. We present a series of numerical examples to demonstrate the performance of this algorithm.

Mathematics subject classifications (MSC2010): 35R30, (65N21)
Keywords: Inverse source problem, inverse scattering, Helmholtz equation, far field splitting, basis pursuit
Short title: Far field splitting by weighted ℓ^1 minimization

1 Introduction

The inverse source problem for time-harmonic acoustic or electromagnetic waves radiated by compactly supported sources attempts to recover information about an unknown source from observations of the radiated wave made at a distance, i.e., from the far field. What makes this problem particularly interesting, apart from its notorious instability, is the non-uniqueness of its solutions without additional assumptions on the unknown source. This necessitates generalized notions of solutions, and over the last several years there has been an increasing interest in alternatives to traditional least squares (see, e.g., [9] for a recent account on the latter). One such alternative is the

*Institut für Mathematik, Universität Würzburg, 97074 Würzburg, Germany (roland.griesmaier@uni-wuerzburg.de)
†Department of Mathematics, University of Washington, Seattle, Washington 98195, U.S.A. (sylvest@uw.edu)

convex scattering support introduced in [20, 21] (see also [22, 24, 25]), which aims to retrieve geometrical properties of the support of the unknown source from its radiated far field. More precisely, the convex scattering support describes the smallest convex set such that any neighborhood of this set supports a source radiating the given far field. This set can not only be computed numerically from far field data, but it also constitutes a rigorously justified lower bound for the convex hull of the support of all solutions to the inverse source problem. On the other hand, the convex scattering support is, by definition, a single convex set, and therefore contains limited topological information. In particular, if a source consists of several well-separated components, the convex scattering support contains no information about the geometric properties of the supports of the individual source components. Utilizing the linearity of the inverse source problem, a possible remedy proposed in [12] is to first decompose the far field radiated by an ensemble of well separated compactly supported sources into the far fields radiated by each of these source components separately, and then to evaluate the convex scattering support of each of these far field components. We call the first step in this procedure the *far field splitting* problem, and the main topic of this work is the development of an efficient numerical algorithm to compute such far field splits. Although inverse source problems and convex scattering supports are our main motivation for considering far field splitting, this inverse problem is clearly of independent interest.

Assuming that the approximate locations of the individual source components are known a priori, we recently discussed in [12] a Galerkin method for the far field splitting problem. More precisely, this algorithm requires the centers and the radii of well separated balls in space containing the supports of the individual source components. Several methods for obtaining this kind of a priori information from far field data are available (see, e.g., [4, 5, 13, 14, 17]). The finite dimensional subspaces used in this Galerkin scheme are spanned by singular vectors of certain "restricted" far field operators associated with the balls containing the individual source components, and the number of degrees of freedom is directly related to the size of these balls. The Galerkin approach has both advantages and shortcomings: It is very fast and highly accurate as long as the balls containing the individual source components given as a priori information are sufficiently small relative to their distances. However, if this is not the case for whatever reasons (e.g., if the a priori information is not sharp), then the Galerkin scheme becomes ill-conditioned and the reconstructions deteriorate.

The aim of the present work is to reduce the dependence of the reconstructed far field components on the accuracy of the given a priori information on the approximate source locations. To this end we replace the Galerkin approach, which was based on an ℓ^2 characterization and may therefore be considered as a finite dimensional least squares best approximation problem, by a weighted ℓ^1 minimization problem in the spirit of basis pursuit (see, e.g., [6]). This strategy reflects the same basic observation as the Galerkin scheme: that far fields radiated by ensembles of compactly supported sources are nearly sparse in certain overcomplete dictionaries that are obtained by merging suitably transformed Fourier bases depending on the source locations. However, instead of selecting a finite number of degrees of freedom based on the given a priori information beforehand, as is done in the Galerkin framework, the sparsity promoting weighted ℓ^1 minimization scheme—at least theoretically—recovers the right dictionary elements automatically, and thus its solution is much less dependent on the accuracy of the a priori information.

The use of suitable weights is crucial to guarantee that the unique solution of the weighted ℓ^1 minimization problem does indeed yield the desired solution of the far field splitting problem. We solve the ℓ^1 minimization problem numerically by applying the iterated soft thresholding algorithm (see, e.g., [8]), which, in particular, accounts for the ill-posedness of the far field splitting problem.

In the second part of this paper, we propose an iterative strategy to successively improve the quality of the weights by solving a sequence of weighted ℓ^1 minimization problems, where the weights used for the next iteration are computed from the value of the current solution (see, e.g., [3] for a related approach). This not only improves the convergence speed of the algorithm but also the quality of the reconstructions significantly. Numerical examples confirm that this iteratively reweighted sparsity promoting far field splitting method requires much less accurate a priori information than the Galerkin scheme from [12].

The splitting of a far field due to an ensemble of sources into individual far field components has already been considered in earlier work [18] (see also [23]). However, the approach proposed in these articles is based on actually reconstructing the individual source components by solving severely ill-posed integral equations. We avoid this additional source of instability by directly working with the far field patterns, and more importantly, we make explicit use of the sparsity properties of Fourier expansions of far fields in our algorithm. Recently, in [15], a method for the separation of time-dependent wave fields due to multiple sources has been proposed, based on absorbing boundary conditions.

The paper is organized as follows. In the next section we review some facts concerning far fields of time-harmonic waves radiated by compactly supported sources and their Fourier analysis. In Section 3 we characterize the smallest ball centered at the origin that supports a source radiating a given far field in terms of a weighted ℓ^1 (rather than ℓ^2) norm of its Fourier coefficients. The far field splitting problem is formulated as a weighted ℓ^1 minimization problem in Section 4. In Section 5 we introduce the *narrow box principle* as a means to estimate the approximate location of a single localized source from its far field pattern. We utilize this principle in Section 6 to develop an iterative reweighting strategy, and then conclude the paper with some final remarks.

2 Far field patterns radiated by compactly supported sources

Suppose that $f \in L^2_0(\mathbb{R}^2)$ represents a compactly supported acoustic or electromagnetic source in the plane. Then the time-harmonic wave $u \in H^1_{\mathrm{loc}}(\mathbb{R}^2)$ radiated by f at *wave number* $\kappa > 0$ solves the *source problem* for the Helmholtz equation

$$-\Delta u - \kappa^2 u \;=\; f \qquad \text{in } \mathbb{R}^2\,, \tag{2.1a}$$

and satisfies the *Sommerfeld radiation condition*

$$\lim_{r\to\infty} \sqrt{r}\Big(\frac{\partial u}{\partial r} - \mathrm{i}\kappa u\Big) \;=\; 0 \qquad \text{for } |x| = r\,. \tag{2.1b}$$

Recalling the *fundamental solution* of the Helmholtz equation in two dimensions

$$\Phi_\kappa(x) \;:=\; \frac{\mathrm{i}}{4}\, H_0^{(1)}(\kappa|x|)\,, \qquad x \in \mathbb{R}^2\,,\; x \neq 0\,,$$

the solution to (2.1) can be written as a volume potential

$$u(x) \;=\; \int_{\mathbb{R}^2} \Phi_\kappa(x-y) f(y)\, \mathrm{d}y\,, \qquad x \in \mathbb{R}^2\,. \tag{2.2}$$

From the asymptotic behavior of Hankel functions for large argument it follows immediately that

$$u(x) \;=\; \frac{e^{\mathrm{i}\pi/4}}{\sqrt{8\pi\kappa}}\, \frac{e^{\mathrm{i}\kappa|x|}}{\sqrt{|x|}}\, u^\infty(\hat{x}) \;+\; O\left(|x|^{-3/2}\right) \qquad \text{as } |x| \to \infty, \tag{2.3}$$

where $\hat{x} := x/|x|$ and

$$u^\infty(\hat{x}) \;=\; \int_{\mathbb{R}^2} e^{-\mathrm{i}\kappa\hat{x}\cdot y} f(y)\,\mathrm{d}y\,, \qquad \hat{x}\in S^1 \tag{2.4}$$

(see, e.g., [7]). The function u^∞ is called the *far field pattern* radiated by f, and accordingly the *far field operator* $\mathcal{F}: L^2_0(\mathbb{R}^2) \to L^2(S^1)$,

$$\mathcal{F}f \;:=\; \hat{f}|_{\kappa S^1}\,, \tag{2.5}$$

where as usual $\hat{f}$ denotes the Fourier transform of f, maps compactly supported sources to their radiated far field patterns.

The inverse source problem aims to recover information about an unknown source $f \in L^2_0(\mathbb{R}^2)$ from observations of the far field pattern $u^\infty = \mathcal{F}f$. It is obvious from (2.5) that the far field operator $\mathcal{F}$ has a non-trivial kernel $\mathcal{N}(\mathcal{F})$. More precisely, using Rellich's lemma and the uniqueness of solutions to (2.1) it can be seen that

$$\mathcal{N}(\mathcal{F}) \;=\; \{g = -\Delta v - \kappa^2 v \mid v \in H^2_0(\mathbb{R}^2)\}\,.$$

The elements of $\mathcal{N}(\mathcal{F})$ are called *non-radiating sources*. In particular, neither the source f nor its support is uniquely determined by the far field pattern u^∞ radiated by f, and since non-radiating sources can have arbitrarily large support, no upper bound for the support is possible. There are, however, well defined notions of lower bounds: We say that a compact set $\Omega \subset \mathbb{R}^2$ *carries* u^∞, if every open neighborhood of Ω supports a source $f \in L^2_0(\mathbb{R}^2)$ that radiates this far field pattern. The *convex scattering support* $\mathscr{C}(u^\infty)$ of u^∞ has been defined in [20] (see also [21, 25]) as the intersection of all compact convex sets that carry u^∞. It has been established that $\mathscr{C}(u^\infty)$ itself carries u^∞. Hence $\mathscr{C}(u^\infty)$ is in fact the smallest convex set with this property, and the convex hull of the support of the "true" source f must contain $\mathscr{C}(u^\infty)$. Furthermore, since two disjoint compact sets with connected complements cannot carry the same far field pattern (cf. [25, Lemma 6]), it follows that $\mathscr{C}(u^\infty)$ intersects any connected component of $\mathrm{supp}(f)$, if the corresponding source component is not non-radiating.

The convex scattering support $\mathscr{C}(u^\infty)$ can be approximated numerically by means of

$$\mathscr{C}(u^\infty) \;\approx\; \bigcap_{l=1}^{L} B_{\rho_l}(\zeta_l)\,,$$

where $\{\zeta_1,\dots,\zeta_L\}$ is a sufficiently large number of suitably chosen points in $\mathbb{R}^2$, and ρ_l, $l=1,\dots,L$, denotes the radius of the smallest ball around ζ_l containing $\mathscr{C}(u^\infty)$. To evaluate this approximation one needs to estimate, based on the far field data, the radius of the smallest ball, centered at a given point, that contains the convex scattering support of the far field pattern. Since reliable numerical estimates of this radius will we be important at several places in this work, we discuss this issue in the following in more detail.

We use polar coordinates $\hat{x} = (\cos t, \sin t)$ and $y = |y|(\cos\varphi_y, \sin\varphi_y)$ with $t, \varphi_y \in [0, 2\pi)$, and recall the Jacobi-Anger expansion

$$e^{\pm\mathrm{i}\kappa\hat{x}\cdot y} \;=\; \sum_{n\in\mathbb{Z}} (\pm\mathrm{i})^n e^{-\mathrm{i}n\varphi_y} J_n(\kappa|y|) e^{\mathrm{i}nt} \tag{2.6}$$

(see, e.g., [7, p. 67]). The Fourier expansion of the far field pattern u^∞ radiated by f is given by

$$u^\infty(\hat{x}) \;=\; \sum_{n\in\mathbb{Z}} a_n e^{\mathrm{i}nt}\,, \qquad \hat{x}\in S^1\,,$$

with

$$a_n \;=\; (-\mathrm{i})^n \int_{\mathbb{R}^2} e^{-\mathrm{i}n\varphi_y} J_n(\kappa|y|) f(y)\;\mathrm{d}y\,, \qquad n\in\mathbb{Z}\,. \tag{2.7}$$

If a source f is supported in the ball $B_r(0)$ of radius $r>0$ centered at the origin, then the inequality below for Bessel functions

$$|J_n(\kappa r)| \;\le\; \begin{cases} 1\,, & |n|\le e\kappa r/2\,,\\ \left(\dfrac{\kappa e r}{2|n|}\right)^{|n|}\,, & |n|\ge e\kappa r/2\,, \end{cases} \qquad n\in\mathbb{Z}\,, \tag{2.8}$$

(cf. Theorem A.1 in [12]) implies that we can obtain a lower bound for κr by identifying the number of Fourier coefficients that are significantly larger than zero. To make this more precise, we introduce, for any bounded domain $\Omega\subset\mathbb{R}^2$, the corresponding *restricted far field operator* $\mathcal{F}_\Omega : L^2(\Omega)\to L^2(S^1)$,

$$(\mathcal{F}_\Omega f)(\hat{x}) \;:=\; \int_\Omega e^{-\mathrm{i}\kappa\hat{x}\cdot y} f(y)\;\mathrm{d}y\,. \tag{2.9}$$

In the special case $\Omega=B_r(0)$ the singular system $(\frac{s_n(\kappa r)}{\kappa}; u_n, v_n)$, $n\in\mathbb{Z}$, of $\mathcal{F}_{B_r(0)}$ is known (cf., e.g., [9]): It is given by

$$s_n^2(\kappa r) \;=\; 2\pi\kappa^2 \int_{B_r(0)} J_n^2(\kappa|x|)\;\mathrm{d}x \tag{2.10a}$$

$$u_n(\hat{x}) \;=\; (1/\sqrt{2\pi})\, e^{\mathrm{i}nt}\,, \qquad \hat{x}=(\cos t,\sin t)\in S^1\,, \tag{2.10b}$$

and

$$v_n(x) \;=\; \frac{\kappa\sqrt{2\pi}}{s_n(\kappa r)}\mathrm{i}^n J_n(\kappa|x|) e^{\mathrm{i}n\varphi_x}, \qquad x=|x|(\cos\varphi_x,\sin\varphi_x)\in B_r(0)\,. \tag{2.10c}$$

Therefore, Picard's theorem (see, e.g., [7, p. 92]) implies that a field pattern u^∞ with Fourier coefficients $(a_n)_{n\in\mathbb{Z}}$ belongs to $\mathcal{R}(\mathcal{F}_{B_r(0)})$ for some $r>0$ if and only if

$$\sum_{n\in\mathbb{Z}} \frac{\kappa^2|a_n|^2}{|s_n(\kappa r)|^2} \;<\; \infty\,. \tag{2.11}$$

However, since estimating the radius

$$\rho \;:=\; \max\{|x| \mid x\in\mathscr{C}(u^\infty)\} \tag{2.12}$$

by verifying the convergence of (2.11) for various radii r is not efficient, we will use a much more tractable numerical criterion based on the following lemma.

Lemma 2.1. *Let $r>0$, denote by $a=(a_n)_{n\in\mathbb{Z}}$ the Fourier coefficients of the far field pattern $u^\infty=\mathcal{F}_{B_r(0)}f$ radiated by $f\in L^2(B_r(0))$, and define*[1]

$$\Delta_{\kappa r,u^\infty} \;:=\; \frac{1}{\kappa}\left(\min_{\mathcal{F}_{B_r(0)}f=u^\infty} \frac{\|f\|_{L^2(B_r(0))}}{\|u^\infty\|_{L^2(S^1)}}\right). \tag{2.13}$$

[1]It is not difficult to check that $\Delta_{\kappa r,u^\infty}$ depends only on the product κr (and on u^∞).

Then, for any $N \in \mathbb{N}$ such that $N+1 \geq e\kappa r/2$ we have the inequality

$$\frac{\sum_{|n|>N} |a_n|^2}{\|a\|_{\ell^2}^2} \leq \Delta_{\kappa r, u^\infty}^2 \, \frac{2\pi^2(\kappa r)^2}{N+2} \Big(\frac{e\kappa r}{2N+2}\Big)^{2N+2}. \tag{2.14}$$

In particular the right hand side of (2.14) decays super-linearly as a function of N in this case.

Proof. We denote by

$$f^*(x) := \begin{cases} 2\pi\kappa^2 \sum_{n\in\mathbb{Z}} \dfrac{a_n}{s_n^2(\kappa r)} \, \mathrm{i}^n e^{\mathrm{i}n\varphi_x} J_n(\kappa|x|)\,, & |x| < r\,, \\ 0 & |x| \geq r\,, \end{cases}$$

the source of minimal L^2 norm supported in $B_r(0)$ that radiates u^∞. The estimate (2.8) implies for all $n \in \mathbb{N}$ that

$$s_n^2(\kappa r) = (2\pi)^2\kappa^2 \int_0^r J_n^2(\kappa\rho)\rho \, \mathrm{d}\rho \leq (2\pi)^2\kappa^2 \int_0^r \Big(\frac{e\kappa\rho}{2n}\Big)^{2n} \rho \, \mathrm{d}\rho = \frac{2\pi^2(\kappa r)^2}{n+1}\Big(\frac{e\kappa r}{2n}\Big)^{2n}, \tag{2.15}$$

and applying Parseval's theorem we obtain

$$\Delta_{\kappa r, u^\infty} = \frac{\|f^*\|_{L^2(B_r(0))}}{\kappa \, \|u^\infty\|_{L^2(S^1)}} = \frac{1}{\sqrt{2\pi}} \frac{\|f^*\|_{L^2(B_r(0))}}{\kappa \, \|a\|_{\ell^2}}.$$

Hence, we find for $N+1 \geq e\kappa r/2$ that

$$\frac{N+2}{2\pi^2(\kappa r)^2}\Big(\frac{2N+2)}{e\kappa r}\Big)^{2N+2} \sum_{|n|>N} |a_n|^2 \leq \sum_{n\in\mathbb{Z}} \frac{|a_n|^2}{s_n^2(\kappa r)} = \frac{1}{2\pi\kappa^2}\|f^*\|_{L^2(B_r(0))}^2 = \Delta_{\kappa r, u^\infty}^2 \, \|a\|_{\ell^2}^2 . \tag{2.16}$$

This shows (2.14). ∎

We assume that $\Delta_{\kappa r, u^\infty} \leq 1/\mu$ for some $\mu > 0$, which can be considered as a regularization of the radius estimation problem which excludes certain degenerate sources[2]. We can immediately use Lemma 2.1 to evaluate lower bounds for the radius ρ from (2.12) by determining the largest value of N such that the left hand side of (2.14) is smaller than some threshold. In particular, this suggests estimating the radius ρ from (2.12) numerically by means of

$$\widetilde{\rho} := \kappa^{-1} \min\Big\{ N \in \mathbb{N} \,\Big|\, \sum_{|n|\leq N} |a_n|^2/\|a\|_{\ell^2}^2 \geq 1-\eta \Big\}, \tag{2.17}$$

where $\eta > 0$ is a sufficiently small threshold parameter (see also [12], where this criterion has already been used successfully in numerical examples).

Sources f that are supported in $B_r(z)$ with $z \neq 0$ can be shifted into $B_r(0)$ using the change of variables $f \mapsto \widetilde{f} = f(\,\cdot\, + z)$. Accordingly, (2.4) implies that the far field pattern $\widetilde{u}^\infty$ radiated by $\widetilde{f}$ satisfies

$$\widetilde{u}^\infty(\hat{x}) = (M_z u^\infty)(\hat{x}), \qquad \hat{x} \in S^1, \tag{2.18}$$

[2]In electro-magnetics, f represents a current distribution, and μ can be interpreted as the energy the source radiates into the far field divided by the energy that must be supplied to construct the source.

where, as before, $u^\infty = \mathcal{F}f$ and $M_z : L^2(S^1) \to L^2(S^1)$ is given by

$$(M_z\phi)(\hat{x}) \;=\; e^{\mathrm{i}\kappa\hat{x}\cdot z}\phi(\hat{x}), \qquad \hat{x} \in S^1\,. \tag{2.19}$$

Therefore, combining (2.18)-(2.19) with (2.17) we can estimate the radius of the smallest ball around an arbitrary point $z \in \mathbb{R}^2$ that contains the convex scattering support of a far field pattern u^∞.

For later reference, we note that writing $z = r_z(\cos\varphi_z, \sin\varphi_z)$ and substituting (2.6) into (2.18) implies that the Fourier coefficients $\widetilde{a} = (\widetilde{a}_m)_{m\in\mathbb{Z}}$ of

$$\widetilde{u}^\infty(\hat{x}) \;=\; \sum_{m\in\mathbb{Z}} \widetilde{a}_m e^{\mathrm{i}mt}\,, \qquad \hat{x} \in S^1\,,$$

are given by

$$\widetilde{a}_m \;=\; \sum_{n\in\mathbb{Z}} \mathrm{i}^{n-m} e^{\mathrm{i}(n-m)\varphi_z} J_{n-m}(\kappa r_z)\, a_n\,, \qquad m \in \mathbb{Z}\,.$$

Accordingly, we define $T_z : \ell^2 \to \ell^2$,

$$(T_z a)_m \;=\; \widetilde{a}_m \;=\; \sum_{n\in\mathbb{Z}} \mathrm{i}^{n-m} e^{\mathrm{i}(n-m)\varphi_z} J_{n-m}(\kappa r_z)\, a_n\,. \tag{2.20}$$

3 Weighted ℓ^1 estimates for the Fourier coefficients of u^∞

Before we consider the far field splitting problem and its formulation as a weighted ℓ^1 minimization problem in Section 4 below, we first discuss a third characterization of far field patterns radiated from a ball of radius r around the origin. This characterization is an ℓ^1 version of the Picard criterion (2.11), which will be used to determine the correct weights for the far field splitting scheme in Section 4.

Assuming that $s > 0$ and $1 \le p \le \infty$, we define

$$\sigma_{p,n}(s) \;:=\; \min\Big\{1, \Big(\frac{2}{p|n|+2}\Big)^{\frac{1}{p}} \Big(\frac{es}{2|n|}\Big)^{|n|}\Big\}\,, \qquad n \in \mathbb{Z}\,, \tag{3.1}$$

and accordingly

$$\ell^p_s \;:=\; \Big\{ a = (a_n)_{n\in\mathbb{Z}} \in \ell^2 \;\Big|\; \Big(\frac{a_n}{\sigma_{p,n}(s)}\Big)_{n\in\mathbb{Z}} \in \ell^p \Big\}\,,$$

which shall be equipped with the norm

$$\|a\|_{\ell^p_s} \;:=\; \Big\| \Big(\frac{a_n}{\sigma_{p,n}(s)}\Big)_{n\in\mathbb{Z}} \Big\|_{\ell^p}\,. \tag{3.2}$$

Furthermore, we note that the representation (2.2) together with the far field expansion (2.3)–(2.4) remains valid for compactly supported sources $f \in L^1_0(\mathbb{R}^2)$, and accordingly the restricted far field operators from (2.9) may be extended to bounded linear operators from $L^1(\Omega)$ to $L^2(S^1)$.

Theorem 3.1. *Let $0 < r < \rho < \infty$, and let $u^\infty \in L^2(S^1)$ with Fourier coefficients $a = (a_n)_{n\in\mathbb{Z}} \in \ell^2$.*

(a) If u^∞ is a far field pattern radiated by a compactly supported source[3] $f \in L^1(B_r(0))$, then its Fourier coefficients satisfy

$$a \in \ell^1_{\kappa\rho}\,. \tag{3.3}$$

[3]Throughout, we identify $f \in L^1(B_r(0))$ with its continuation to $\mathbb{R}^2$ by zero whenever appropriate.

(b) On the other hand, if $a \in \ell^1_{\kappa\rho}$, then

$$f(x) \;=\; \begin{cases} 2\pi\kappa^2 \displaystyle\sum_{n\in\mathbb{Z}} \frac{a_n}{s_n^2(\kappa\rho)}\, \mathrm{i}^n e^{\mathrm{i}n\varphi_x} J_n(\kappa|x|)\,, & |x| < \rho\,, \\ 0 & |x| \geq \rho\,, \end{cases} \tag{3.4}$$

is well defined, $f \in L^1(B_\rho(0))$, and f radiates u^∞.

The proof of Theorem 3.1 relies on the following three lemmas:

Lemma 3.2. *Let $1 \leq p, q \leq \infty$ such that $\frac{1}{p} + \frac{1}{q} = 1$, let $0 < r < \infty$, and assume that $u^\infty \in L^2(S^1)$ is a far field pattern radiated by a source $f \in L^q(B_r(0))$. Then the Fourier coefficients $(a_n)_{n\in\mathbb{Z}}$ of u^∞ satisfy*

$$|a_n| \;\leq\; (\pi r^2)^{\frac{1}{p}} \sigma_{p,n}(\kappa r) \|f\|_{L^q(B_r(0))}\,, \qquad n \in \mathbb{Z}\,. \tag{3.5}$$

Proof. Recalling (2.7) and applying Hölder's inequality we find that

$$|a_n| \;\leq\; \int_{B_r(0)} |J_n(\kappa|y|)||f(y)|\,\mathrm{d}y \;\leq\; \|J_n(\kappa|\cdot|)\|_{L^p(B_r(0))} \|f\|_{L^q(B_r(0))}\,.$$

Furthermore, the estimate (2.8) for Bessel functions yields

$$\begin{aligned} \|J_n(\kappa|\cdot|)\|^p_{L^p(B_r(0))} \;&=\; 2\pi \int_0^r |J_n(\kappa r)|^p r\,\mathrm{d}r \\ &\leq\; 2\pi \int_0^r \min\left\{1, \left(\frac{e\kappa r}{2|n|}\right)^{|n|}\right\}^p r\,\mathrm{d}r \\ &\leq\; 2\pi \min\left\{\frac{r^2}{2}, \left(\frac{e\kappa r}{2|n|}\right)^{|n|p} \frac{r^2}{p|n|+2}\right\} \;=\; \pi r^2 \big(\sigma_{p,n}(\kappa r)\big)^p\,. \end{aligned}$$

Combining these estimates we obtain (3.5). ☐

Lemma 3.3. *Let $1 \leq p, q \leq \infty$, and let $0 < r < \rho < \infty$. Then the weights $\sigma_{p,n}(\kappa r)$ and $\sigma_{q,n}(\kappa\rho)$, $n \in \mathbb{Z}$, from (3.1) satisfy*

$$\sum_{n\in\mathbb{Z}} \frac{\sigma_{p,n}(\kappa r)}{\sigma_{q,n}(\kappa\rho)} \;<\; \infty\,.$$

Proof. Recalling the definition of the weights $\sigma_{p,n}(\kappa r)$ an $\sigma_{q,n}(\kappa\rho)$ in (3.1) we can estimate

$$\sum_{|n|\geq \frac{e\kappa\rho}{2}} \frac{\sigma_{p,n}(\kappa r)}{\sigma_{q,n}(\kappa\rho)} \;=\; 2^{\frac{1}{p}-\frac{1}{q}} \sum_{|n|\geq \frac{e\kappa\rho}{2}} \left(\frac{r}{\rho}\right)^{|n|} \frac{(q|n|+2)^{1/q}}{(p|n|+2)^{1/p}} \;\leq\; C \sum_{n\in\mathbb{Z}} |n| \left(\frac{r}{\rho}\right)^{|n|} \;<\; \infty\,.$$

Here and throughout, C denotes a generic positive constant which may be different at different occurrences. ☐

Lemma 3.4. *Let $0 < r < \infty$, and denote by $s_n(\kappa r)$, $n \in \mathbb{Z}$, the rescaled singular values of the restricted far field operator $\mathcal{F}_{B_r(0)}$ from (2.10). Then there exists $C > 0$ independent of n such that*

$$\kappa r \sigma_{1,n}(\kappa r) \;\leq\; C s_n(\kappa r) \qquad \text{for all } n \in \mathbb{Z}\,. \tag{3.6}$$

Proof. Combining (2.10) and the asymptotic behavior of the Bessel functions J_n for large order,

$$|J_n(\kappa r)| \;=\; \frac{1}{\sqrt{2\pi|n|}}\left(\frac{\kappa e r}{2|n|}\right)^{|n|}\left(1+O\Big(\frac{1}{|n|}\Big)\right) \qquad \text{for } |n|\to\infty$$

(cf., e.g., [7, p. 65]), we find that

$$s_n^2(\kappa r) \;=\; (2\pi\kappa)^2\int_0^r\Big(\frac{e\kappa\rho}{2|n|}\Big)^{2|n|}\frac{1}{2\pi|n|}\Big(1+\mathcal{O}\Big(\frac{1}{|n|}\Big)\Big)\rho\,\mathrm{d}\rho \;=\; \frac{2\pi}{|n|}\Big(\frac{e\kappa r}{2|n|}\Big)^{2|n|}\frac{(\kappa r)^2}{2|n|+2}\Big(1+\mathcal{O}\Big(\frac{1}{|n|}\Big)\Big)$$

for $|n|\to\infty$. Therefore,

$$\Big(\frac{\kappa r\sigma_{1,n}(\kappa r)}{s_n(\kappa r)}\Big)^2 \;=\; \frac{4}{\pi}\,\frac{|n|(|n|+1)}{(|n|+2)^2}\Big(1+\mathcal{O}\Big(\frac{1}{|n|}\Big)\Big) \qquad \text{for } |n|\to\infty\,,$$

i.e., the left hand side of this equation is uniformly bounded with respect to $n\in\mathbb{Z}$. This shows (3.6). □

Proof of Theorem 3.1. Suppose that $u^\infty\in L^2(S^1)$ is radiated by a source $f\in L^1(B_r(0))$. Then, using Lemma 3.2 we see that its Fourier coefficients $a=(a_n)_{n\in\mathbb{Z}}$ satisfy

$$\sum_{n\in\mathbb{Z}}\Big|\frac{a_n}{\sigma_{1,n}(\kappa\rho)}\Big| \;=\; \sum_{n\in\mathbb{Z}}\frac{|a_n|}{\sigma_{\infty,n}(\kappa r)}\frac{\sigma_{\infty,n}(\kappa r)}{\sigma_{1,n}(\kappa\rho)} \;\le\; \|f\|_{L^1(B_r(0))}\sum_{n\in\mathbb{Z}}\left|\frac{\sigma_{\infty,n}(\kappa r)}{\sigma_{1,n}(\kappa\rho)}\right|.$$

Applying Lemma 3.3 we thus obtain (3.3).

Conversely, let $a\in\ell^1_{\kappa\rho}$ and define f by (3.4). Using the Cauchy-Schwarz inequality, (2.10), and Lemma 3.4 we find that

$$\begin{aligned}
\|f\|_{L^1(B_\rho(0))} &\le 2\pi\kappa^2\sum_{n\in\mathbb{Z}}\frac{|a_n|}{s_n^2(\kappa\rho)}\int_{B_\rho(0)}|J_n(\kappa|x|)|\,\mathrm{d}x\\
&\le 2\pi\kappa^2\sum_{n\in\mathbb{Z}}\frac{|a_n|}{s_n^2(\kappa\rho)}|B_\rho(0)|^{1/2}\Big(\int_{B_\rho(0)}J_n^2(\kappa|x|)\,\mathrm{d}x\Big)^{1/2}\\
&= \sqrt{2}\pi\kappa\rho\sum_{n\in\mathbb{Z}}\frac{|a_n|}{s_n(\kappa\rho)} \;\le\; C\sum_{n\in\mathbb{Z}}\frac{|a_n|}{\sigma_{1,n}(\kappa\rho)} \;<\; \infty\,.
\end{aligned}$$

This shows that $f\in L^1(B_\rho(0))$. From the singular value decomposition of the restricted far field operator $\mathcal{F}_{B_\rho(0)}$ in (2.10) together with the boundedness of the continuous extension of $\mathcal{F}_{B_\rho(0)}$ from $L^1(B_\rho(0))$ to $L^2(S^1)$, it is now obvious that f from (3.4) radiates the far field pattern with the Fourier coefficients a. □

4 Splitting far field patterns by weighted ℓ^1 minimization

Henceforth, we assume that the far field pattern u^∞ in (2.4) is a superposition

$$u^\infty \;=\; u_1^\infty+\cdots+u_m^\infty \tag{4.1}$$

of m far field patterns $u_1^\infty, \dots, u_m^\infty$ that are radiated by well separated compactly supported sources. By this we mean that there exist disjoint balls $B_{r_1}(z_1), \dots, B_{r_m}(z_m)$ with $|z_j - z_l| \gg r_j + r_l$ for $1 \le j, l \le m$, $j \ne l$ and sources $f_j \in L^2(B_{r_j}(z_j))$, $j = 1, \dots, m$, such that $\mathcal{F}_{B_{r_j}(z_j)} f_j = u_j^\infty$.

We seek to recover the individual far field components $u_1^\infty, \dots, u_m^\infty$ from (possibly noisy) observations of u^∞, together with the *a priori* information that each of the convex scattering supports $\mathscr{C}(u_j^\infty)$ lies inside the corresponding[4] $B_{r_j}(z_j)$. We call this the *far field splitting* problem.

It follows immediately that the decomposition in (4.1) is uniquely determined, since for any two bounded domains $\Omega_1, \Omega_2 \subset \mathbb{R}^2$ such that $\mathbb{R}^2 \setminus \Omega_1$ and $\mathbb{R}^2 \setminus \Omega_2$ are connected and $\overline{\Omega_1} \cap \overline{\Omega_2} = \emptyset$ the intersection of the ranges of the corresponding restricted far field operators is trivial, i.e.,

$$\mathcal{R}(\mathcal{F}_{\Omega_1}) \cap \mathcal{R}(\mathcal{F}_{\Omega_2}) \;=\; \{0\}$$

(cf., e.g., [25, Lemma 6]). On the other hand, as a consequence of the one-to-one correspondance between Herglotz wave functions and their kernels ([7, Thm. 3.15]), both $\mathcal{F}_{\Omega_1}$ and $\mathcal{F}_{\Omega_1}$ have dense range, which indicates that the far field splitting problem is ill-posed without further assumptions.

In [12] we developed a Galerkin scheme to recover $u_1^\infty, \dots, u_m^\infty$ from the given data u^∞ and $B_{r_1}(z_1), \dots, B_{r_m}(z_m)$. This algorithm evaluates approximations $v_j^\infty \in V_j \subset L^2(S^1)$ of u_j^∞, $j = 1, \dots, m$, satisfying

$$\langle v_1^\infty + \cdots + v_m^\infty, \phi \rangle_{L^2(S^1)} \;=\; \langle u^\infty, \phi \rangle_{L^2(S^1)} \qquad \text{for all } \phi \in V_1 \oplus \cdots \oplus V_m \,, \tag{4.2}$$

where the finite dimensional Galerkin subspaces V_j, $j = 1, \dots, m$, are spanned by the left singular vectors of the restricted far field operators $\mathcal{F}_{B_{r_j}(z_j)}$ corresponding to the $2N_j + 1$ largest singular values (cf. (2.10)). We chose $N_j = \lceil \alpha \kappa r_j \rceil$ for some fixed $\alpha > 0$ as cut-off parameter, which reflects the superlinear decay of the Fourier coefficients of u_j^∞ for $|n| \gtrsim \kappa r_j$ (cf. (2.14)). In other words,

$$V_j \;=\; \{ M_{z_j}^* u_n \mid |n| \le N_j \} \,, \qquad j = 1, \dots, m \,,$$

where M_{z_j} is the multiplication operator from (2.19) and $(u_n)_{n \in \mathbb{Z}}$ denotes the Fourier basis of $L^2(S^1)$. In [12] we provided an error analysis for this algorithm, and we showed that it is fairly well conditioned, as long as the relative distances between the balls $B_{r_1}(z_1), \dots, B_{r_m}(z_m)$, describing the given a priori information on the approximate location and size of the unknown convex scattering supports $\mathscr{C}(u_1^\infty), \dots, \mathscr{C}(u_m^\infty)$, are large with respect to their radii.

A drawback of this scheme is the sensitivity of its approximations with respect to the accuracy of the required a priori information. In numerical tests we observed that the method works very well if the balls $B_{r_1}(z_1), \dots, B_{r_m}(z_m)$ are well separated and relatively close to $\mathscr{C}(u_1^\infty), \dots, \mathscr{C}(u_m^\infty)$, respectively. However, if the radii $r_1, \dots, r_m$ are chosen too large or if the points $z_1, \dots, z_m$ are too far away from the barycenters of the individual convex scattering supports, then the accuracy of the approximations deteriorates, even if the $\mathscr{C}(u_1^\infty), \dots, \mathscr{C}(u_m^\infty)$ are well separated and thus the Galerkin scheme with more accurate a priori information would be well conditioned. In the following we discuss a more robust approach to far field splitting that in particular can handle much less accurate a priori information.

If the balls $B_{r_1}(z_1), \dots, B_{r_m}(z_m)$ are well separated, then the dimensions of the Galerkin subspaces $V_1, \dots, V_m$ are small relative to the number of Fourier modes needed to accurately represent

[4] The convex scattering support $\mathscr{C}(u_j^\infty)$, $j = 1, \dots, m$, is a subset of any convex set and thus in particular of any ball that carries u_j^∞.

the whole far field pattern u^∞ (a rough estimate for the latter is given by $\kappa \max_{j=1,\dots,m}(|z_j| + r_j)$). Therefore the decomposition of u^∞ obtained in (4.2) can be considered as a sparse approximation of the far field pattern u^∞ in the overcomplete dictionary

$$\mathcal{D} \;=\; \{M^*_{z_1} u_n \mid n \in \mathbb{Z}\} \cup \cdots \cup \{M^*_{z_m} u_n \mid n \in \mathbb{Z}\}\,. \tag{4.3}$$

Basis pursuit (see, e.g., [6]) is a method for finding such a sparse decomposition without choosing the relevant dictionary elements in advance. Applied to the far field splitting problem with the dictionary from (4.3), basis pursuit means solving the constrained optimization problem

$$\text{minimize} \sum_{j=1}^m \|b_j\|_{\ell^1} \quad \text{subject to} \quad \sum_{j=1}^m T^*_{z_j} b_j \;=\; a\,, \tag{4.4}$$

where as before $a = (a_n)_{n\in\mathbb{Z}}$ denotes the Fourier coefficients of u^∞, and T_{z_j}, $j = 1, \dots, m$, are the convolution operators from (2.20). However, a generic solution $\boldsymbol{b} = [b_1, \dots, b_m] \in \ell^2 \times \cdots \times \ell^2$ of (4.4) need not represent a valid far field split, since one or more of the far fields given by the Fourier series

$$v^\infty_j(\hat{x}) \;=\; \sum_{n\in\mathbb{Z}} T^*_{z_j} b_j \, e^{\mathrm{i}nt}\,, \qquad \hat{x} = (\cos(t), \sin(t)) \in S^1\,,$$

may not be in the range of the corresponding restricted far field operator $\mathcal{F}_{B_{r_j}(z_j)}$, $1 \le j \le m$, respectively. In fact, it might not even be a far field pattern radiated by any compactly supported source. Hence we modify (4.4), and replace the ℓ^1 norms by weighted ℓ^1 norms with weight functions chosen as in (3.2). We will show that this is sufficient to obtain a constrained optimization problem that is genuinely equivalent to the original far field splitting problem.

Given u^∞ and $B_{r_1}(z_1), \dots, B_{r_m}(z_m)$ as above, we choose $\rho_j > r_j$, $1 \le j \le m$, such that $\overline{B_{\rho_j}(z_j)} \cap \overline{B_{\rho_l}(z_l)} = \emptyset$ for $1 \le j, l \le m$, $j \ne l$ and consider the constrained optimization problem

$$\text{minimize} \sum_{j=1}^m \|b_j\|_{\ell^1_{\kappa\rho_j}} \quad \text{subject to} \quad \sum_{j=1}^m T^*_{z_j} b_j \;=\; a\,. \tag{4.5}$$

The following proposition shows that (4.5) has a unique solution, which yields a valid far field split.

Proposition 4.1. *Suppose that u^∞ is a superposition of m far field patterns $u^\infty_1, \dots, u^\infty_m$ that are radiated from well separated balls $B_{r_1}(z_1), \dots, B_{r_m}(z_m)$, and denote by $a = (a_n)_{n\in\mathbb{Z}}$ the Fourier coefficients of u^∞. Then the constrained minimization problem (4.5) with $\rho_j > r_j$, $j = 1, \dots, m$, such that $\overline{B_{\rho_j}(z_j)} \cap \overline{B_{\rho_l}(z_l)} = \emptyset$ for $1 \le j, l \le m$, $j \ne l$ has a unique solution $\boldsymbol{b}^\dagger = [b^\dagger_1, \dots, b^\dagger_m] \in \ell^1_{\kappa\rho_1} \times \cdots \times \ell^1_{\kappa\rho_m}$, and this solution satisfies*

$$u^\infty_j(\hat{x}) \;=\; \sum_{n\in\mathbb{Z}} T^*_{z_j} b^\dagger_j \, e^{\mathrm{i}nt}\,, \qquad \hat{x} = (\cos(t), \sin(t)) \in S^1\,,\; j = 1, \dots, m\,.$$

Proof. Let $1 \le j \le m$, and let a_j be the sequence of Fourier coefficients of u^∞_j. Since u^∞_j is radiated from $B_{r_j}(z_j)$ it follows by translation that $M_{z_j} u^\infty_j$ is radiated from $B_{r_j}(0)$, and thus the first part of Theorem 3.1 shows that the Fourier coefficients $b_j = T_{z_j} a_j$ of $M_{z_j} u^\infty_j$ satisfy $b_j \in \ell^1_{\kappa\rho_j}$. Hence there exists at least one admissible $\boldsymbol{b} = [b_1, \dots, b_m] \in \ell^1_{\kappa\rho_1} \times \cdots \times \ell^1_{\kappa\rho_m}$ that satisfies the constraint of (4.5).

On the other hand, the second part of Theorem 3.1 implies that for any admissible $\boldsymbol{b} = [b_1, \dots, b_m] \in \ell^1_{\kappa\rho_1} \times \cdots \times \ell^1_{\kappa\rho_m}$ satisfying the constraint of (4.5) the sequences $T^*_{z_1} b_1, \dots, T^*_{z_m} b_m$ are the Fourier coefficients of a solution to the far field splitting problem with $B_{r_1}(z_1), \dots, B_{r_m}(z_m)$ replaced by $B_{\rho_1}(z_1), \dots, B_{\rho_m}(z_m)$. Since these are unique, we find that (4.5) has a unique solution. □

Alternatively, if only perturbed observations $u^{\infty,\delta}$ of the true far field data u^∞ are available, and these observations satisfy

$$\|u^\infty - u^{\infty,\delta}\|_{L^2(S^1)} \le \delta \qquad \text{and} \qquad \|u^{\infty,\delta}\|_{L^2(S^1)} > \delta \tag{4.6}$$

for some $\delta > 0$, then the Fourier coefficients $a^\delta = (a^\delta_j)_{j\in\mathbb{Z}}$ of $u^{\infty,\delta}$ satisfy $\|a - a^\delta\|_{\ell^2} \le \delta/\sqrt{2\pi}$ and $\|a^\delta\|_{\ell^2} > \delta/\sqrt{2\pi}$. Accordingly, we modify (4.5) and consider the constrained optimization problem

$$\text{minimize} \sum_{j=1}^m \|b_j\|_{\ell^1_{\kappa\rho_j}} \quad \text{subject to} \quad \Big\| a^\delta - \sum_{j=1}^m T^*_{z_j} b_j \Big\|_{\ell^2} \le \delta/\sqrt{2\pi}\,. \tag{4.7}$$

It is well known that (4.7) is equivalent to minimizing the Tikhonov functional[5]

$$\Psi_{\alpha,\boldsymbol{\rho}}(\boldsymbol{b}) = \Big\| a^\delta - \sum_{j=1}^m T^*_{z_j} b_j \Big\|^2_{\ell^2} + \alpha \sum_{j=1}^m \|b_j\|_{\ell^1_{\kappa\rho_j}}\,, \qquad \boldsymbol{b} = [b_1, \dots, b_m] \in \ell^2 \times \cdots \times \ell^2\,, \tag{4.8}$$

for a suitably chosen regularization parameter $\alpha > 0$ (see, e.g., [11, Prop. 2.2]).

Before we discuss the existence and uniqueness of minimizers of $\Psi_{\alpha,\rho}$, we introduce as a short hand notation the operator $K : \ell^2 \times \cdots \times \ell^2 \to \ell^2$,

$$K\boldsymbol{b} = \sum_{j=1}^m T^*_{z_j} b_j\,, \tag{4.9}$$

and note that its adjoint $K^* : \ell^2 \to \ell^2 \times \cdots \times \ell^2$ is given by

$$K^* c = [T_{z_1} c, \dots, T_{z_m} c]\,.$$

Since the convolution operators $T^*_{z_j}$, $j = 1, \dots, m$, from (2.20) are ℓ^2 isometries, the operator norm of K is bounded by[6] $\|K\| \le \sqrt{m}$, and therefore $\|K^*K\|_{\ell^2\times\cdots\times\ell^2} \le m$. Choosing $0 < \omega < 1/m$ such that $\|\omega K^* K\| < 1$, it follows immediately from [8, Prop. 2.1] that any minimizer $\boldsymbol{b}^* = [b^*_1, \dots, b^*_1]$ of the Tikhonov functional $\Psi_{\alpha,\boldsymbol{\rho}}$ from (4.8) satisfies the fixed point equation

$$\boldsymbol{b}^* = \boldsymbol{S}_{\omega\alpha,\boldsymbol{\rho}}(\boldsymbol{b}^* + \omega K^*(a - K\boldsymbol{b}^*))\,, \tag{4.10}$$

where the non-linear thresholding function $\boldsymbol{S}_{\omega\alpha,\boldsymbol{\rho}}$ is defined componentwise by

$$\boldsymbol{S}_{\omega\alpha,\boldsymbol{\rho}}\boldsymbol{b} = [S_{\omega\alpha,\rho_1} b_1, \dots, S_{\omega\alpha,\rho_m} b_m]\,, \qquad \boldsymbol{b} = [b_1, \dots, b_m] \in \ell^2 \times \cdots \times \ell^2\,,$$

[5] In (4.8) the index $\boldsymbol{\rho}$ stands for $[\rho_1, \dots, \rho_m]$.

[6] We consider the norm $\|(a_1, \dots, a_m)\|_{\ell^2\times\cdots\times\ell^2} = \big(\sum_{j=1}^m \|a_j\|^2_{\ell^2}\big)^{\frac{1}{2}}$ on $\ell^2 \times \cdots \times \ell^2$.

with

$$(S_{\omega\alpha,\rho_j} b_j)_n \;=\; \begin{cases} \left(|b_{j,n}| - \dfrac{\omega\alpha}{2\sigma_{1,n}(\kappa\rho_j)}\right) e^{\mathrm{i}\arg(b_{j,n})} & \text{if } |b_{j,n}| \geq \frac{\omega\alpha}{2\sigma_{1,n}(\kappa\rho_j)}\,, \\ 0 & \text{if } |b_{j,n}| < \frac{\omega\alpha}{2\sigma_{1,n}(\kappa\rho_j)}\,, \end{cases} \qquad n \in \mathbb{Z}\,,$$

for $j = 1, \ldots, m$. (cf. [8, Remark 2.5]). In particular, minimizers of $\Psi_{\alpha,\boldsymbol{\rho}}$ have only finitely many nonzero coefficients, and therefore two minimizers of $\Psi_{\alpha,\boldsymbol{\rho}}$ have to coincide except for possibly finitely many coefficients.

Although the operator K of (4.9) is clearly not injective, we show in the next lemma that its restriction to any finite dimensional subspace has trivial null space. This property is often called *finite basis injectivity* (see, e.g., [2]), and together with what we have seen so far, it guarantees uniqueness for the minimizer of $\Psi_{\alpha,\boldsymbol{\rho}}$.

Lemma 4.1. *Let $z_1, \ldots, z_m$ be distinct points in $\mathbb{R}^2$. Then the restriction of the operator K from (4.9) to any finite dimensional subspace of $\ell^2 \times \cdots \times \ell^2$ is injective.*

Proof. Let $b_1, \ldots, b_m \in \ell^2$ such that each b_j, $j = 1, \ldots, m$, has only finitely many non-zero coefficients and suppose that

$$T^*_{z_1} b_1 + \cdots + T^*_{z_m} b_m \;=\; 0\,. \tag{4.11}$$

Then, with $s_n^2(\kappa r)$, $n \in \mathbb{Z}$, denoting the rescaled singular values of the restricted far field operator $\mathcal{F}_{B_r(0)}$ from (2.10), the sources

$$f_j(x) \;=\; \begin{cases} 2\pi\kappa^2 \displaystyle\sum_{n\in\mathbb{Z}} \frac{b_{j,n}}{s_n^2(\kappa r)}\, \mathrm{i}^n e^{\mathrm{i}n\varphi_{x-z_j}} J_n(\kappa|x-z_j|)\,, & |x-z_j| < r\,, \\ 0\,, & |x-z_j| \geq r\,, \end{cases} \qquad j = 1, \ldots, m\,,$$

are well defined and have disjoint supports for some sufficiently small value of $r > 0$. Moreover, it follows immediately from (2.10) that f_j, $j = 1, \cdots, m$, radiates the far field pattern

$$v_j^\infty(\hat{x}) \;=\; \sum_{m\in\mathbb{Z}} (T^*_{z_j} b_j)_m e^{\mathrm{i}mt}\,, \qquad \hat{x} = (\cos t, \sin t) \in S^1\,,$$

respectively. Since (4.11) implies that $v_1^\infty + \cdots + v_m^\infty = 0$, the fact that two disjoint bounded domains with connected complement cannot carry the same far field implies that $b_1 = \cdots = b_m = 0$. □

Corollary 4.2. *Suppose that u^∞ is a superposition of m far field patterns $u_1^\infty, \ldots, u_m^\infty$ that are radiated from well separated balls $B_{r_1}(z_1), \ldots, B_{r_m}(z_m)$, and denote by $a = (a_n)_{n\in\mathbb{Z}}$ the Fourier coefficients of u^∞. Then for any $\alpha > 0$ the unconstrained minimization problem*

$$\text{minimize } \Psi_{\alpha,\boldsymbol{\rho}}(\boldsymbol{b}) \;=\; \Big\| a^\delta - \sum_{j=1}^m T^*_{z_j} b_j \Big\|^2_{\ell^2} + \alpha \sum_{j=1}^m \|b_j\|_{\ell^1_{\kappa\rho_j}} \quad \text{over} \quad \boldsymbol{b} \in \ell^2 \times \cdots \times \ell^2\,, \tag{4.12}$$

with $\rho_j > r_j$, $j = 1, \ldots, m$, such that $\overline{B_{\rho_j}(z_j)} \cap \overline{B_{\rho_l}(z_l)} = \emptyset$ for $1 \leq j, l \leq m$, $j \neq l$, has a unique solution $\boldsymbol{b}^*_{\alpha,\boldsymbol{\rho}} \in \ell^1_{\kappa\rho_1} \times \cdots \times \ell^1_{\kappa\rho_m}$ satisfying (4.10) for any $0 < \omega < 1/m$.

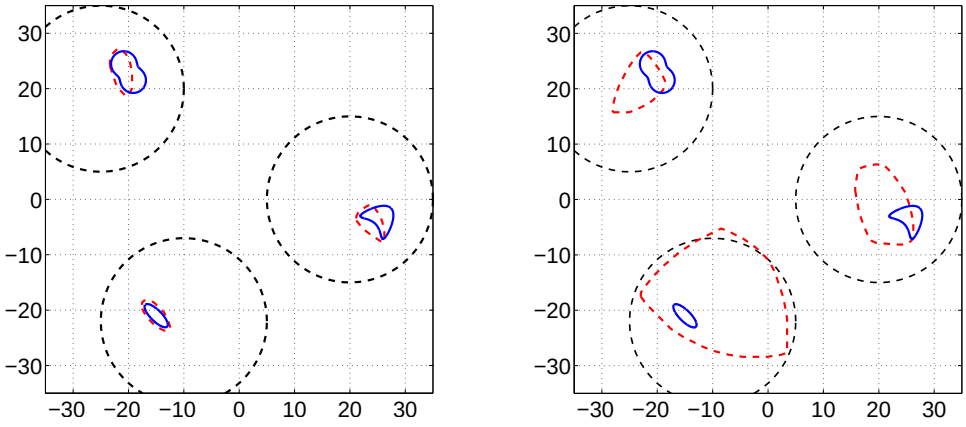

Figure 4.1: Left: Geometry of the scatterers (solid lines), convex scattering supports of u_1^∞, u_2^∞, and u_3^∞ (dashed lines), and a priori guess for the source locations (dashed circles). Right: Same as left but with convex scattering supports of v_1^∞, v_2^∞, and v_3^∞ from Example 4.3 (dashed lines)

Although $\boldsymbol{b}^*_{\alpha,\boldsymbol{\rho}}$ does of course not solve (4.5) exactly, the corresponding Fourier series

$$v_j^\infty(\hat{x}) \;=\; \sum_{n\in\mathbb{Z}} T^*_{z_j} b_j \, e^{\mathrm{i}nt}\,, \qquad \hat{x} = (\cos(t),\sin(t)) \in S^1\,,\;\; j = 1,\dots,m\,,$$

are at least in the range of $\mathcal{F}_{B_{r_j}(z_j)}$, respectively. Moreover, it can be shown that (4.12) together with an appropriate parameter choice rule $\alpha = \alpha(\delta, u^{\infty,\delta})$ constitutes a convergent regularization method (see, e.g., [8, 10, 11]), i.e.,

$$\lim_{\delta\to 0}\Big(\sup_{\|u^\infty - u^{\infty,\delta}\|_{L^2(S^1)}\le\delta} \big\|\boldsymbol{b}^*_{\alpha(\delta,u^{\infty,\delta}),\boldsymbol{\rho}} - \boldsymbol{b}^\dagger\big\|_{\ell^2}\Big) \;=\; 0\,.$$

In our numerical computations we solve (4.12) for fixed $\alpha > 0$, by applying the iterative soft thresholding algorithm from [8]. Choosing $0 < \omega < 1/m$ and an initial guess $\boldsymbol{b}^{(0)} \in \ell^2 \times \cdots \times \ell^2$ (e.g., $\boldsymbol{b}^{(0)} = (0,\dots,0)$), the corresponding sequence of iterates is given by

$$\boldsymbol{b}^{(k+1)} \;=\; \boldsymbol{S}_{\omega\alpha,\boldsymbol{\rho}}(\boldsymbol{b}^{(k)} + \omega K^*(a^\delta - K\boldsymbol{b}^{(k)}))\,, \qquad k = 0,1,\dots\,. \tag{4.13}$$

If follows from [8, Thm. 3.1] that $(\boldsymbol{b}^{(k)})_{k\in\mathbb{N}}$ converges strongly to the unique minimizer $\boldsymbol{b}^*_{\alpha,\boldsymbol{\rho}}$ of $\Psi_{\alpha,\boldsymbol{\rho}}$, regardless of the choice of $\boldsymbol{b}^{(0)}$.

Example 4.3. To illustrate this weighted ℓ^1 far field splitting algorithm, we consider a scattering problem with three obstacles (an ellipse, a nut, and a kite) as shown in Figure 4.1 The three obstacles are illuminated by an incoming plane wave $u^i(x) = e^{\mathrm{i}\kappa x\cdot d}$, $x \in \mathbb{R}^2$, with incident direction $d = (1,0)$ and wave number $\kappa = 5$. Assuming that the ellipse is sound soft whereas the kite and the nut are sound hard, the scattered field u^s satisfies the homogeneous Helmholtz equation outside the obstacles together with the Sommerfeld radiation condition at infinity and Neumann (for the ellipse) or Dirichlet boundary conditions (for the kite and the nut) on the boundaries of the obstacles. We note that the same example has been used in [12, Sect. 7] to test the Galerkin scheme for the far field splitting problem and hence, the results can easily be compared.

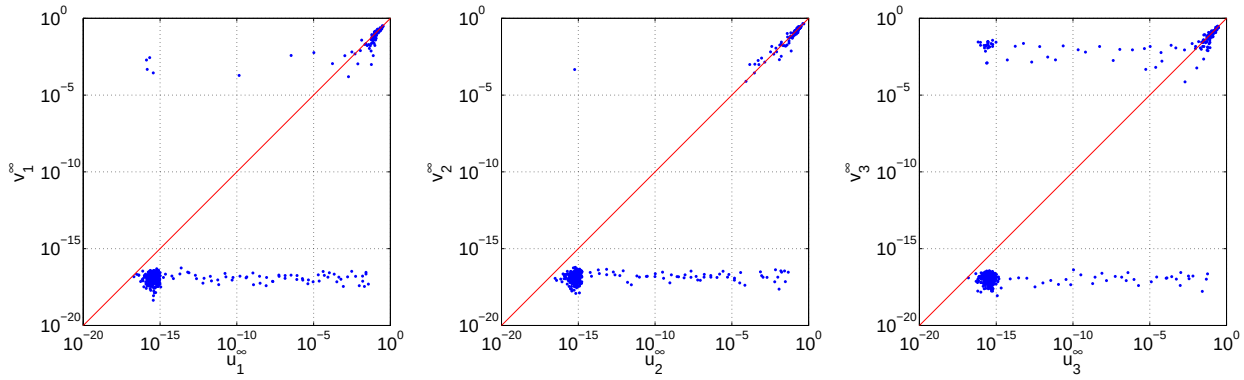

Figure 4.2: Scatter plots of the absolute values of the Fourier coefficients of v_j^∞ vs. u_j^∞ for $j = 1, 2, 3$ ($\omega = 1/4$, $\alpha = 10^{-2}$, 10^4 iterations).

It is well known that the far field pattern u^∞ of u^s can be written as a superposition of three far field patterns u_1^∞, u_2^∞, u_3^∞ radiated by three individual smooth sources supported in arbitrarily small neighborhoods of the three scatterers, respectively (cf., e.g., [21, Lemma 3.6]). In our computations the exact far field pattern u^∞ has been simulated on an equidistant grid with 512 points on the unit circle using the Nyström method as described in [7, 19]. As a byproduct this implementation also provides access to the exact far field components u_j^∞, $j = 1, 2, 3$. Using lighter dashed lines we include in Figure 4.1 (left) the boundaries of the convex scattering supports $\mathscr{C}(u_j^\infty)$, $j = 1, 2, 3$, of these exact far field components, which have been evaluated numerically using the implementation of the convex scattering support described in [12, Sect. 7].

We apply the iterative soft thresholding procedure (4.13) to compute approximations v_j^∞ of u_j^∞, $j = 1, 2, 3$. To this end we use $\boldsymbol{b}^{(0)} = (0, \ldots, 0)$ as initial guess, and we choose $\omega = 1/4$ and $\alpha = 10^{-2}$ for the regularization parameter. We use the dashed circles shown in Figure 4.1 as a priori information on the approximate source locations $B_{r_j}(z_j)$, $j = 1, 2, 3$, and we choose $\rho_j = r_j$, $j = 1, 2, 3$, in the Tikhonov functional $\Psi_{\alpha,\boldsymbol{\rho}}$ from (4.8). More precisely, $z_1 = (20, 0)$, $z_2 = (-25, 20)$, $z_3 = (-10, -22)$, and $r_1 = r_2 = r_3 = 15$. This a priori information is considerably less accurate than the a priori guess used in [12, Sect. 7]. Our stability analysis from [12] indicates that the Galerkin scheme from [12] is severely ill-conditioned for these less accurate a priori data, and numerical tests confirm that the Galerkin algorithm does not give useful reconstructions. In fact, the condition number of the corresponding linear system is 6.1×10^{15}.

The absolute values of the approximations of the Fourier coefficients of v_j^∞ obtained by the iterative soft thresholding algorithm after 10^4 iterations are plotted against the absolute values of the Fourier coefficients of the exact far field components u_j^∞ for $j = 1, 2, 3$ in Figure 4.2. While the reconstructions of the largest Fourier coefficients of the individual far field components is relatively decent, the smaller Fourier coefficients are still not recovered well. Accordingly the convex scattering supports $\mathscr{C}(v_j^\infty)$, $j = 1, 2, 3$, of these approximate far field components shown in Figure 4.1 (right) do not yield satisfactory reconstructions of the locations and shapes of the unknown scatterers. However, the results are much better than the corresponding results obtained with the Galerkin scheme from [12], where almost all reconstructed Fourier coefficients of the corresponding approximation v_j^∞ in the index range $-e\kappa r_j/2 \le n \le e\kappa r_j/2$ are of order one. This is the expected behavior for an ℓ^2 based reconstruction scheme, and it illustrates the advantage of the sparsity

promoting weighted ℓ^1 approach.

Finally, we note that, due to the notoriously slow convergence of the iterative soft thresholding algorithm, further iterations do not change the results significantly. ◊

We observed in Example 4.3 that the numerical results obtained by solving the minimization problem (4.12) given inaccurate a priori information on the approximate source locations are better than the corresponding results for the Galerkin scheme from [12] with the same a priori information, but still may not be satisfactory. Therefore, in the following sections we combine the minimization problem (4.12) with an iterative reweighting strategy that aims to gradually improve the quality of the available a priori information by solving a sequence of weighted ℓ^1 minimization problems, and incorporating information on the source locations obtained from the value of the current solution in the next iteration. To this end we need an algorithm to estimate the centers and the radii of balls $B_{r_j}(z_j)$ containing the convex scattering supports $\mathscr{C}(v_j^\infty)$ of the current approximations v_j^∞, $j = 1, \ldots, m$. This is the subject of the next section.

5 The narrow box principle

In Section 2 we observed that the Fourier coefficients $a = (a_n)_{n\in\mathbb{Z}}$ of the far field pattern u^∞ radiated by a not too exotic source $f \in L_0^2(B_r(z))$ are essentially supported in the index range $|n| \lesssim \kappa(r+|z|)$. Clearly, moving the origin closer to the source by shifting z into the origin as in (2.18)-(2.20), makes this index range smaller. Accordingly, the magnitudes of the Fourier coefficients $\widetilde{a}_n = (T_z a)_n$, $|n| \lesssim \kappa r$, should on average exceed the magnitudes of the Fourier coefficients a_n, $|n| \lesssim \kappa(r + |z|)$, since the corresponding transformation T_z from (2.20) is ℓ^2 unitary.

In the following we formalize this *narrow box principle* and discuss some simple consequences.

Theorem 5.1. *Let u^∞ be the far field pattern radiated by a compactly supported source $f \in L^2(B_r(z))$ with $z \in \mathbb{R}^2$ and $r > 0$, denote by $a = (a_n)_{n\in\mathbb{Z}}$ the Fourier coefficients of u^∞, and let $\Delta_{\kappa r,u^\infty}$ be as defined in (2.13). Then the following hold:*

(a) Suppose $1 \le q \le 2$. The inequality

$$1 \le \frac{\|T_z a\|_{\ell^q}}{\|T_z a\|_{\ell^2}} \le (2N+1)^{\frac{1}{q}-\frac{1}{2}} \left(1 + 2^{\frac{1}{q}} (2\pi^2 \kappa r)^{\frac{1}{2}} \left(\frac{e\kappa r}{2N}\right)^N \Delta_{\kappa r,u^\infty}\right) \tag{5.1}$$

is valid for all $N \in \mathbb{N}$ satisfying $N \ge e\kappa r/2$.

(b) Suppose $2 \le q \le \infty$. The inequality

$$1 \le \frac{\|T_z a\|_{\ell^2}}{\|T_z a\|_{\ell^q}} \le (2N+1)^{\frac{1}{2}-\frac{1}{q}} \left(1 - (2\pi^2 \kappa r)^{\frac{1}{2}} \left(\frac{e\kappa r}{2N}\right)^N \Delta_{\kappa r,u^\infty}\right)^{-1} \tag{5.2}$$

is valid for all $N \in \mathbb{N}$ satisfying $N \ge e\kappa r/2$.

Proof. As before, we denote by $\widetilde{a} := (\widetilde{a}_n)_{n\in\mathbb{Z}} = T_z a$ the Fourier coefficients of the shifted far field pattern $M_z u^\infty$.

We first consider the case $1 \le q \le 2$, and note that

$$\|\widetilde{a}\|_{\ell^q} \le \Big(\sum_{|n|\le N} |\widetilde{a}_n|^q\Big)^{\frac{1}{q}} + \Big(\sum_{|n|>N} |\widetilde{a}_n|^q\Big)^{\frac{1}{q}}. \tag{5.3}$$

Hölder's inequality implies that the first term on the right hand side of (5.3) can be estimated by

$$\sum_{|n|\le N} |\widetilde{a}_n|^q \;\le\; (2N+1)^{1-\frac{q}{2}}\Big(\sum_{|n|\le N} |\widetilde{a}_n|^2\Big)^{\frac{q}{2}} \;\le\; (2N+1)^{1-\frac{q}{2}}\|\widetilde{a}\|_{\ell^2}^q\,. \tag{5.4}$$

Combining Hölder's inequality with (2.16) and (2.15) gives an estimate for the second term on the right hand side of (5.3), i.e.

$$\begin{aligned}
\sum_{|n|>N} |\widetilde{a}_n|^q &= \sum_{k=0}^{\infty}\sum_{|n|=N2^k+1}^{N2^{k+1}} |\widetilde{a}_n|^q \;\le\; \sum_{k=0}^{\infty}(2N2^k)^{1-\frac{q}{2}}\Big(\sum_{|n|=N2^k+1}^{N2^{k+1}} |\widetilde{a}_n|^2\Big)^{\frac{q}{2}} \\
&\le \sum_{k=0}^{\infty}(2N2^k)^{1-\frac{q}{2}}\Delta_{\kappa r,u^\infty}^q s_{N2^k+1}^q(\kappa r)\|\widetilde{a}\|_{\ell^2}^q \\
&\le (2N)^{1-\frac{q}{2}}\Delta_{\kappa r,u^\infty}^q\,\|\widetilde{a}\|_{\ell^2}^q \sum_{k=0}^{\infty} 2^{k(1-\frac{q}{2})}\Big(\frac{2\pi^2(\kappa r)^2}{N2^k+2}\Big(\frac{e\kappa r}{2(N2^k+1)}\Big)^{2(N2^k+1)}\Big)^{\frac{q}{2}}\,.
\end{aligned}$$

Assuming that $N \ge e\kappa r/2$, we can further estimate

$$\begin{aligned}
&\sum_{|n|>N} |\widetilde{a}_n|^q \\
&\le \Big((2N)^{\frac{1}{q}-\frac{1}{2}}\Delta_{\kappa r,u^\infty}\Big(\frac{2\pi^2(\kappa r)^2}{N}\Big)^{\frac{1}{2}}\Big(\frac{e\kappa r}{2N}\Big)^N\|\widetilde{a}\|_{\ell^2}\Big)^q \sum_{k=0}^{\infty} 2^{k(1-(2+N2^k)q)}\Big(\frac{e\kappa r}{2N}\Big)^{(N(2^k-1)+1)q} \\
&\le \Big((2N)^{\frac{1}{q}-\frac{1}{2}}\Delta_{\kappa r,u^\infty}(2\pi^2\kappa r)^{\frac{1}{2}}\Big(\frac{e\kappa r}{2N}\Big)^N\|\widetilde{a}\|_{\ell^2}\Big)^q \sum_{k=0}^{\infty} 2^{-k} \\
&\le \Big(2^{\frac{1}{q}}(2N+1)^{\frac{1}{q}-\frac{1}{2}}\Delta_{\kappa r,u^\infty}(2\pi^2\kappa r)^{\frac{1}{2}}\Big(\frac{e\kappa r}{2N}\Big)^N\|\widetilde{a}\|_{\ell^2}\Big)^q\,.
\end{aligned} \tag{5.5}$$

Combining (5.3)–(5.5) yields the upper bound in (5.1). To obtain the lower bound, we note that Parseval's theorem, Hölder's inequality, and the Hausdorff-Young inequality imply that

$$\|\widetilde{a}\|_{\ell^2} \;=\; (2\pi)^{-\frac{1}{2}}\|M_z u^\infty\|_{L^2(S^1)} \;\le\; (2\pi)^{-\frac{1}{p}}\|M_z u^\infty\|_{L^p(S^1)} \;\le\; \|\widetilde{a}\|_{\ell^q}\,. \tag{5.6}$$

In order to prove the second statement we proceed similarly. Assuming $2 \le q \le \infty$, we note that

$$\|\widetilde{a}\|_{\ell^2} \;\le\; \Big(\sum_{|n|\le N} |\widetilde{a}_n|^2\Big)^{\frac{1}{2}} + \Big(\sum_{|n|>N} |\widetilde{a}_n|^2\Big)^{\frac{1}{2}}\,, \tag{5.7}$$

and use Hölder's inequality to estimate the first term on the right hand side of (5.7), obtaining

$$\sum_{|n|\le N} |\widetilde{a}_n|^2 \;\le\; (2N+1)^{1-\frac{2}{q}}\|\widetilde{a}\|_{\ell^q}^2\,. \tag{5.8}$$

The second term on the right hand side of (5.7) can be estimated with the aid of (2.16) and (2.15),

$$\sum_{|n|>N} |\widetilde{a}_n|^2 \;\le\; s_{N+1}^2(\kappa r)\Delta_{\kappa r,u^\infty}^2\|\widetilde{a}\|_{\ell^2}^2 \;\le\; \frac{2\pi^2(\kappa r)^2}{N+2}\Big(\frac{e\kappa r}{2N+2}\Big)^{2N+2}\Delta_{\kappa r,u^\infty}^2\|\widetilde{a}\|_{\ell^2}^2\,.$$

For $N \geq e\kappa r/2$, this implies that

$$\sum_{|n|>N} |\widetilde{a}_n|^2 \;\leq\; \Big((2\pi^2\kappa r)^{\frac{1}{2}} \Big(\frac{e\kappa r}{2N}\Big)^N \Delta_{\kappa r, u^\infty} \|\widetilde{a}\|_{\ell^2} \Big)^2 . \tag{5.9}$$

Combining (5.7)–(5.9) yields the upper bound in (5.2). The lower bound then follows by applying the Hausdorff-Young inequality, Hölder's inequality, and Parseval's theorem,

$$\|T_z a\|_{\ell^q} \;\leq\; (2\pi)^{-\frac{1}{p}} \|M_z u^\infty\|_{L^p(S^1)} \;\leq\; (2\pi)^{-\frac{1}{2}} \|M_z u^\infty\|_{L^2(S^1)} \;\leq\; \|T_z a\|_{\ell^2} \,. \tag{5.10}$$

This ends the proof of the theorem. □

To illustrate the estimates (5.1) and (5.2) from Theorem 5.1, we consider the special case of a far field pattern radiated by a single point source. Although point sources are not square integrable, similar estimates can be obtained by slightly modifying the arguments of the proof of Theorem 5.1.

Example 5.2. The far field pattern u^∞ radiated by a point source $f = \delta_z$ at $z = r_z(\cos\phi_z, \sin\phi_z) \in \mathbb{R}^2$ is given by

$$u^\infty(\hat{x}) \;=\; e^{-\mathrm{i}\kappa \hat{x}\cdot z} \;=\; \sum_{n\in\mathbb{Z}} a_n e^{-\mathrm{i}nt} \,, \qquad \hat{x} = (\cos t, \sin t) \in S^1 \,,$$

with Fourier coefficients

$$a_n \;=\; a_n(z) \;=\; (-\mathrm{i})^n e^{-\mathrm{i}n\phi_z} J_n(\kappa r_z)$$

(cf. (2.6)). Accordingly, the sequence $a(z) = (a_n(z))_{n\in\mathbb{Z}}$ satisfies

$$\|a(z)\|_{\ell^q} \;=\; \begin{cases} \sum_{n\in\mathbb{Z}} |J_n(\kappa r_z)|^q \,, & 1 \leq q < \infty \,, \\ \sup_{n\in\mathbb{Z}} |J_n(\kappa r_z)| \,, & q = \infty \,. \end{cases}$$

The estimates (5.4) and (5.8) for the lower order Fourier coefficients a_n, $|n| \leq N$, as well as the lower bounds (5.6) and (5.10), carry over to the setting considered in this example without changes. On the other hand, assuming $N \geq \lceil e\kappa r_z - 1 \rceil$, the estimate (2.8) implies that

$$\sum_{|n|>N} |a_n|^q \;=\; \sum_{|n|>N} |J_n(\kappa r_z)|^q \;\leq\; \sum_{|n|>N} 2^{-q|n|} \;=\; 2\frac{2^{-q(N+1)}}{1-2^{-q}} \,, \qquad 1 \leq q \leq 2 \,.$$

Recalling that $\|a\|_{\ell^2} = \|(J_n(r))_{n\in\mathbb{Z}}\|_{\ell^2} = 1$ (see, e.g., [1, 9.1.76]) and choosing $N = \lceil e\kappa r - 1 \rceil$, we obtain that

$$1 \;\leq\; \|a(z)\|_{\ell^q} \;\leq\; (2\lceil e\kappa r_z \rceil - 1)^{\frac{1}{q}-\frac{1}{2}} + \frac{2^{\frac{1}{q}} 2^{-\lceil e\kappa r_z \rceil}}{(1-2^{-q})^{\frac{1}{q}}} \,, \qquad 1 \leq q \leq 2 \,, \tag{5.11}$$

$$1 \;\leq\; \frac{1}{\|a(z)\|_{\ell^q}} \;\leq\; (2\lceil e\kappa r_z \rceil - 1)^{\frac{1}{2}-\frac{1}{q}} + \frac{2^{\frac{1}{2}} 2^{-\lceil e\kappa r_z \rceil}}{(1-2^{-2})^{\frac{1}{2}}} \frac{1}{\|a(z)\|_{\ell^q}} \,, \qquad 2 \leq q \leq \infty \,. \tag{5.12}$$

These estimates should be compared to (5.1) and (5.2).

In Figure 5.1 we plot $\|a(z)\|_{\ell^1} = \|(J_n(\kappa r_z))_{n\in\mathbb{N}}\|_{\ell^1}$ (left) and $1/\|a(z)\|_{\ell^4} = 1/\|(J_n(\kappa r_z))_{n\in\mathbb{N}}\|_{\ell^4}$ (right) as a function of $r_z \in [0, 10]$ for $\kappa = 5$ (solid line). Note that these functions have a two-scale behavior: They are monotonically increasing on a macroscopic scale, but also contain high frequency

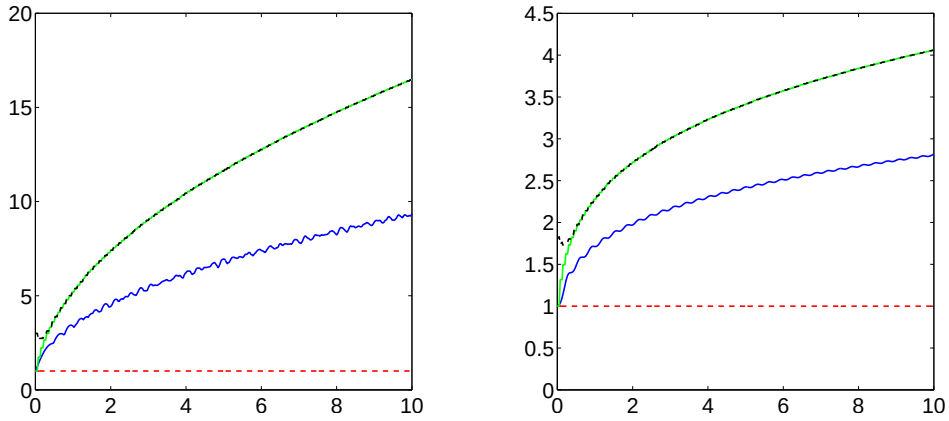

Figure 5.1: Left: $\|(J_n(\kappa r_z))_{n\in\mathbb{N}}\|_{\ell^1}$ (solid) and the bounds of (5.11) (dashed) versus r_z for $\kappa = 5$. Right: $1/\|(J_n(\kappa r_z))_{n\in\mathbb{N}}\|_{\ell^4}$ (solid) and the bounds of (5.12) (dashed) versus r_z for $\kappa = 5$.

oscillations with small amplitude on the micro scale. The dashed lines in these plots correspond to the lower and upper bounds from (5.11) (left) and (5.12) (right). The first term on the right hand side of these estimates is included as lighter solid curve in Figure 5.1. Although the bounds are clearly not sharp, they give at least the right qualitative behavior. The second term in the upper bounds in (5.11) and (5.12) diminishes quickly away from the origin. ◊

The estimates (5.1) and (5.2) immediately suggest a numerical procedure for approximating the center z and the radius r_z of the smallest ball $B_{r_z}(z)$ containing the convex scattering support $\mathscr{C}(u^\infty)$ of the far field pattern u^∞ radiated by a single localized source f: First use (2.17) to determine an approximation $\widetilde{\rho}_0$ of the radius of the smallest circle around the origin enclosing $\mathscr{C}(u^\infty)$. This gives a preliminary rough estimate of a region of interest containing $\mathscr{C}(u^\infty)$. Then, again denoting the Fourier coefficients of u^∞ by $a = (a_n)_{n\in\mathbb{Z}}$, evaluate

$$\widetilde{z} \;=\; \operatorname{argmin}_{y\in B_{\widetilde{\rho}_0}(0)} \|T_y a\|_{\ell^q} \qquad\qquad \text{for some } 1 \le q < 2 \tag{5.13a}$$

or

$$\widetilde{z} \;=\; \operatorname{argmax}_{y\in B_{\widetilde{\rho}_0}(0)} \|T_y a\|_{\ell^q} \qquad\qquad \text{for some } 2 < q \le \infty\,. \tag{5.13b}$$

According to (5.1) and (5.2), this point $\widetilde{z}$ should be close to $\mathscr{C}(u^\infty)$. Finally, apply (2.17) to $T_{\widetilde{z}}a$ to determine an approximation $\widetilde{\rho}_{\widetilde{z}}$ of the radius of the smallest ball around $\widetilde{z}$ that contains $\mathscr{C}(u^\infty)$. The ball $B_{\widetilde{\rho}_{\widetilde{z}}}(\widetilde{z})$ constitutes a new approximation of $B_{r_z}(z)$.

Example 5.3. To illustrate this algorithm we again consider the scattering problem with three obstacles illuminated by a single plane wave incident field from the left that has been introduced in Example 4.3. For $j = 1, 2, 3$ we denote the Fourier coefficients of the exact far field component u_j^∞ by $a^{(j)} = (a_n^{(j)})_{n\in\mathbb{Z}}$, and show in Figure 5.2 gray scale images of $\|T_y a^{(j)}\|_{\ell^1}$ (left) and $\|T_y a^{(j)}\|_{\ell^4}$ (right) locally around the corresponding scatterers. More precisely, these figures contain plots of $\|T_y a^{(j)}\|_{\ell^1}$ and $\|T_y a^{(j)}\|_{\ell^4}$ for $y \in B_{r_j}(z_j)$, $j = 1, 2, 3$, where the balls $B_{r_j}(z_j)$ coincide with the priori information on the approximate source location used in Example 4.3. These visualizations confirm that the position of the minimum of $\|T_y a^{(j)}\|_{\ell^1}$ and of the maximum of $\|T_y a^{(j)}\|_{\ell^4}$ is quite close to the position of jth scatterer for each $j = 1, 2, 3$.

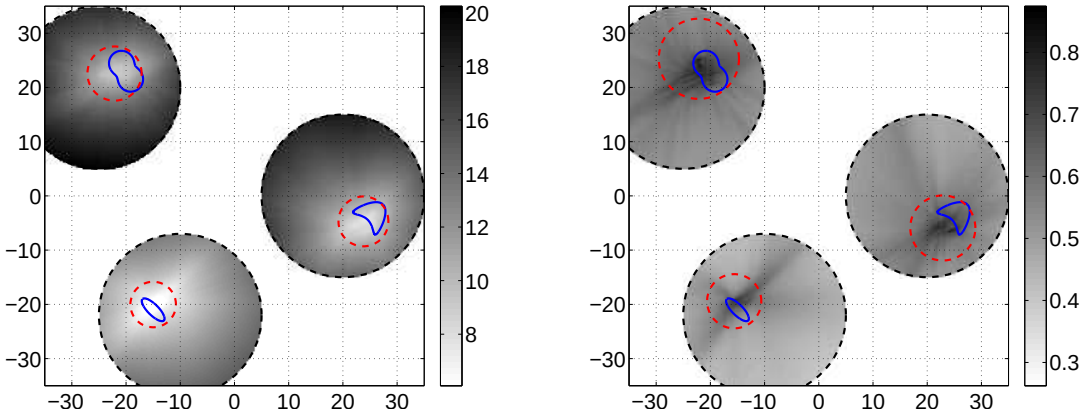

Figure 5.2: Left: $\|T_y a^{(j)}\|_{\ell^1}$, $j = 1, 2, 3$ (gray scale), approximation of the source location $B_{\widetilde{\rho}_{\widetilde{z}}}(\widetilde{z})$ (dashed), and geometry of the scatterers (solid). Right: $\|T_y a^{(j)}\|_{\ell^4}$, $j = 1, 2, 3$ (gray scale), approximation of the source location $B_{\widetilde{\rho}_{\widetilde{z}}}(\widetilde{z})$ (dashed), and geometry of the scatterers (solid).

As in (5.13), we denote the positions of these minima or maxima by $\widetilde{z}_j$, $j = 1, 2, 3$, and apply (2.17) with threshold parameter $\eta = 10^{-4}$ to the transformed Fourier coefficients $T_{\widetilde{z}_j} a^{(j)}$ to approximate the radius of the smallest ball around $\widetilde{z}_j$ containing $\mathscr{C}(u_j^\infty)$. The corresponding circles $B_{\widetilde{\rho}_{\widetilde{z}}}(\widetilde{z})$, $j = 1, 2, 3$, are shown in Figure 5.2 (dashed lines) together with the geometry of the true scatterers (solid lines). It can be seen that this procedure significantly improves the quality of the a priori information on the approximate source locations from Example 4.3. The results are slightly better for the ℓ^1 norm than for the ℓ^4 norm. We note that the picture on the right does not change much, if we replace the ℓ^4 norm by the ℓ^∞ norm. ◊

6 Iteratively reweighted ℓ^1 far field splitting

Having shown how to estimate the center and the radius of the smallest ball containing the convex scattering support of a given far field pattern radiated by a single localized source numerically, we now combine this procedure with the weighted ℓ^1 minimization algorithm for the far field splitting problem from Section 4. The aim is to successively improve the given a priori information on the approximate source locations that determines the weights used in the minimization problem (4.12) by solving a sequence of these weighted ℓ^1 minimization problems, where the a priori information used for the next iteration is computed from the value of the current solution. Improving the a priori information on the approximate source locations also enhances the stability of the splitting algorithm and thus, it improves the quality of the reconstructions.

In Algorithm 6.1 we describe this reweighting strategy in more detail. In our numerical computations we solve the constrained minimization problem in step 5 as before by applying the iterated soft shrinkage procedure from (4.13) to approximate a minimizer of the corresponding Tikhonov functional from (4.12). In step 6 of the algorithm we use the criterion (5.13) with $q = 1$ to update the a priori information z_j, $j = 1, \ldots, m$, on the approximate source locations, since this ℓ^1 criterion usually gave the best results in our numerical tests. When updating r_j, $j = 1, \ldots, m$, we prevent increasing radii by comparing the new estimate with the radius used in the previous step of the iteration. We note that there is no guarantee that none of these balls $B_{r_j}(z_j)$ is too small, i.e.,

Algorithm 6.1 Far field splitting by iteratively reweighted ℓ^1 minimization

Suppose noisy observations $u^{\infty,\delta}$ of $u^\infty = u_1^\infty + \cdots + u_m^\infty$ where $u_1^\infty, \ldots, u_m^\infty$ are radiated from $B_{r_1}(z_1), \ldots, B_{r_m}(z_m)$, respectively, satisfying (4.6) are given.

1: **function** $[v_1^\infty, \ldots, v_m^\infty] = \textsc{Splitting}\,(u^{\infty,\delta}, \delta, \kappa, z_1, \ldots, z_m, r_1, \ldots, r_m)$

2: Compute the Fourier coefficients of $u^{\infty,\delta}$ and store the result in a^δ.

3: Set $z_j^{(0)} = z_j$ and $r_j^{(0)} = r_j$ for $j = 1, \ldots, m$.

4: **for** $l = 0, 1, 2, \ldots$ **do**

5: Compute

$$\boldsymbol{b}^{(l)} \;=\; \operatorname{argmin}\Big(\sum_{j=1}^m \|b_j^{(l)}\|_{\ell^1_{\kappa r_j^{(l)}}}\Big) \quad \text{subject to} \quad \Big\|a^\delta - \sum_{j=1}^m T^*_{z_j^{(l)}} b_j\Big\|_{\ell^2} \;\le\; \delta/\sqrt{2\pi}\,.$$

6: Update a priori information: For $j = 1, \ldots, m$ compute

$$z_j^{(l+1)} \;=\; z_j^{(l)} + \operatorname{argmin}_{y \in B_{r_j^{(l)}}(0)} \|T_y b_j^{(l)}\|_{\ell^1}\,.$$

Choose a threshold parameter $0 < \eta < 1$, evaluate for $j = 1, \ldots, m$ the expression

$$\widetilde{\rho}_j \;:=\; \kappa^{-1} \min\Big\{N \in \mathbb{N} \;\Big|\; \sum_{|n| \le N} |b_{j,n}^{(l)}|^2 / \|b_j\|_{\ell^2}^2 \;\ge\; 1 - \eta\Big\}$$

from (2.17), and set

$$r_j^{(l+1)} \;=\; \min\{r_j^{(l)}\,,\; \widetilde{\rho}_j\}\,.$$

7: Terminate on convergence or when l attains a specific max. number of iterates $l_{\max}$.

8: **end for**

9: The entries of $T^*_{z_1^{(l)}} b_1^{(l)}, \ldots, T^*_{z_m^{(l)}} b_m^{(l)}$ are the Fourier coefficients of the far field components $v_1^\infty, \ldots, v_l^\infty$, respectively.

10: **end function**

smaller than the corresponding convex scattering support $\mathscr{C}(u_j^\infty)$ after this update, but using an appropriate threshold parameter η in (2.17) we did not observe such a behavior in our numerical tests.

Typically a small number of iterations in the overall procedure is sufficient to obtain a very good estimates for the balls $B_{r_1}(z_1), \ldots, B_{r_m}(z_m)$ containing the individual source components, and thus to enhance the reconstructions of the ℓ^1 far field splitting procedure significantly. However, since even with very good a priori information the iterative soft shrinkage still converges rather slowly, we propose to apply the Galerkin scheme from [12] as a final post processing step using the accurate a priori information obtained in the last step of the iteration in Algorithm 6.1. This then typically yields highly accurate results.

Example 6.1. We return to the scattering problem with three obstacles from Example 4.3, and apply Algorithm 6.1 to compute approximations v_j^∞ of the individual far field components u_j^∞, $j = 1, 2, 3$. We start with the same a priori information as used in Example 4.3 (cf. Figure 4.1), and solve the constrained optimization problems in step 5 of Algorithm 6.1 using the iterated soft thresholding procedure from (4.13) with initial guess $\boldsymbol{b}^{(0)} = (0, \ldots, 0)$, $\omega = 1/4$, and regularization parameter $\alpha = 10^{-3}$. We stop each iterative thresholding procedure after 10^3 iterations. Then

Iteration counter	Centers			Radii		
l	$z_1^{(l)}$	$z_2^{(l)}$	$z_3^{(l)}$	$r_1^{(l)}$	$r_2^{(l)}$	$r_3^{(l)}$
0	$(20.0, -0.0)$	$(-25.0, 20.0)$	$(-10.0, -22.0)$	15.0	15.0	15.0
1	$(22.0, -5.0)$	$(-23.3, 22.6)$	$(-14.4, -20.0)$	13.6	10.6	15.0
2	$(22.9, -4.9)$	$(-22.2, 22.3)$	$(-14.5, -19.9)$	5.4	6.0	4.6
3	$(24.2, -4.2)$	$(-21.2, 23.4)$	$(-14.6, -20.0)$	5.0	5.4	4.4
4	$(24.2, -4.2)$	$(-21.3, 23.4)$	$(-14.6, -20.0)$	4.6	5.2	4.0
5	$(24.2, -4.2)$	$(-21.2, 23.4)$	$(-14.7, -20.0)$	4.4	5.2	3.8
10	$(24.2, -4.2)$	$(-21.3, 23.4)$	$(-14.6, -20.0)$	4.0	5.2	3.8
20	$(24.2, -4.2)$	$(-21.2, 23.4)$	$(-14.7, -20.0)$	4.0	5.2	3.8

Table 1: Convergence history of updates of the a priori information on the approximate source locations.

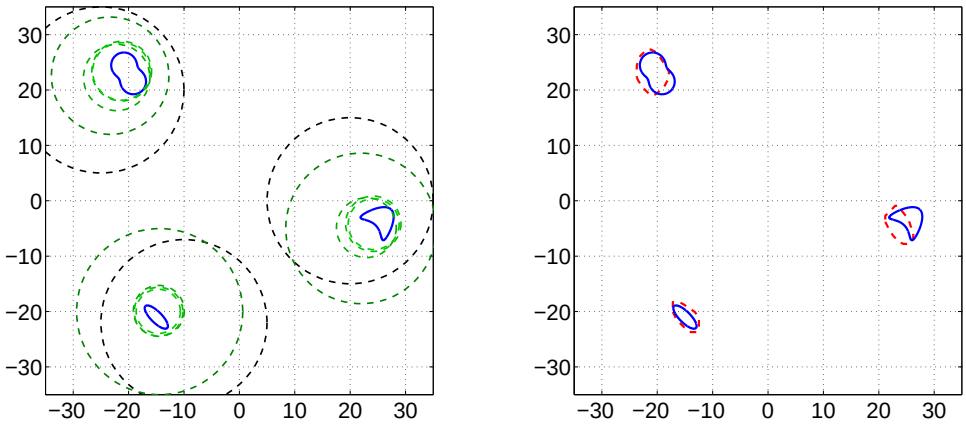

Figure 6.1: Left: Convergence history of the updated a priori information on the source locations (dashed circles) and geometry of the scatterers (solid lines). Right: Convex scattering supports of v_1^∞, v_2^∞, and v_3^∞ (dashed lines) and geometry of the scatterers (solid lines).

we update the estimates for the centers and radii of the disks containing the individual source components as outlined in step 6 of Algorithm 6.1, using the thresholding parameter $\eta = 10^{-4}$.

The convergence history of the successively improved a priori information is shown in Table 1. We observe that the quality of the updated a priori information improves rather quickly. After 10 iterations the estimates for the centers and radii become stationary for this example. The corresponding disks $B_{r_j^{(l)}}(z_j^{(l)})$, $l = 0, \ldots, 5$, are also shown as dashed circles in Figure 6.1 (left). We note that already a very small number of iterations in the overall procedure is sufficient to improve the given a priori information in this example substantially.

The absolute values of the approximations of the Fourier coefficients of v_j^∞ obtained by Algorithm 6.1 after 5 iterations with 10^3 iterated soft thresholding steps each, are plotted against the absolute values of the Fourier coefficients of the exact far field components u_j^∞ for $j = 1, 2, 3$ in Figure 6.2. The reconstructions of the largest Fourier coefficients of the individual far field components are significantly better than the corresponding results without reweighting from Example 4.3. Using this approximate far field split we compute the convex scattering supports $\mathscr{C}(v_j^\infty)$, $j = 1, 2, 3$, of the individual far field components shown in Figure 6.1 (right). Comparing these reconstructions

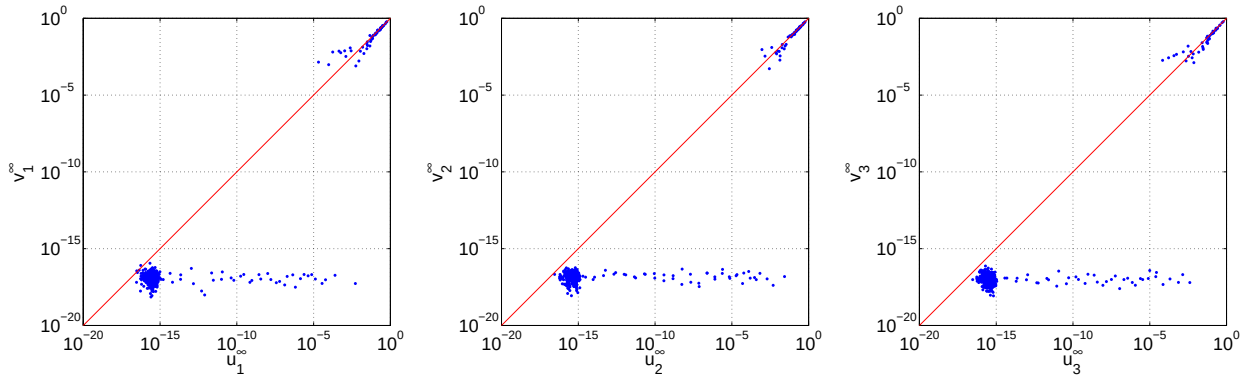

Figure 6.2: Scatter plots of the absolute values of the Fourier coefficients of v_j^∞ vs. u_j^∞ for $j = 1, 2, 3$ ($\omega = 1/4$, $\alpha = 10^{-2}$, $\eta = 10^{-4}$, after 5 iterations in Algorithm 6.1 with 10^3 iterated soft thresholding steps each).

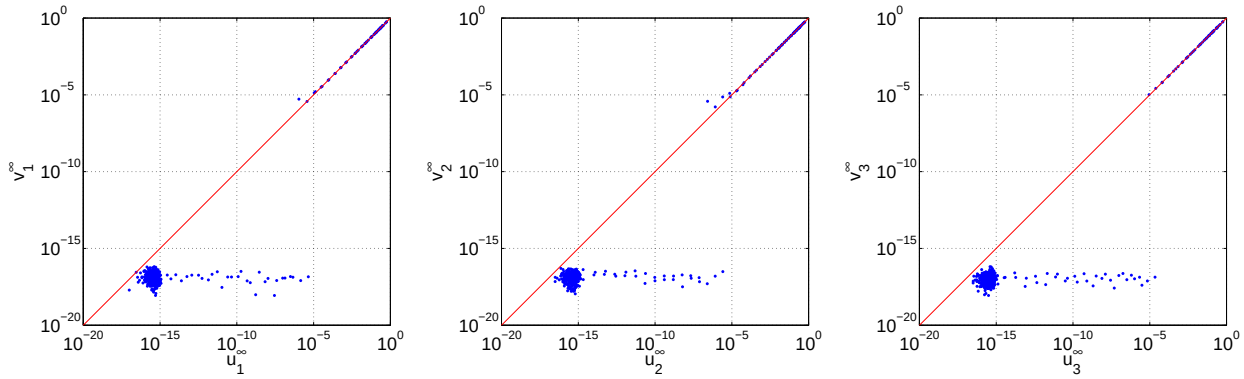

Figure 6.3: Scatter plots of the absolute values of the Fourier coefficients of v_j^∞ vs. u_j^∞ for $j = 1, 2, 3$ (Galerkin scheme using the improved a priori information after 5 iterations in Algorithm 6.1).

with the convex scattering supports $\mathscr{C}(u_j^\infty)$, $j = 1, 2, 3$, of the exact far field components shown in Figure 4.1 (left) and with the convex scattering supports $\mathscr{C}(v_j^\infty)$, $j = 1, 2, 3$, of the approximate far field components obtained without reweighting in Example 4.3 and shown in Figure 4.1 (right) confirms that the far field splits obtained with Algorithm 6.1 allow for significantly improved reconstructions of the supports of the unknown scatterers in this example.

We note that the overall computational costs of Algorithm 6.1 in this example are actually lower than in Example 4.3, where we considered 10^4 iterations in the soft thresholding procedure, whereas here we have 5×10^3 soft thresholding iterations plus 5 updates of the a priori information on the approximate source locations.

Using the improved a priori information obtained after 5 iterations in Algorithm 6.1, we compute an even more accurate far field split by applying the Galerkin method from [12] as a post processing step. The absolute values of the corresponding approximations of the Fourier coefficients of v_j^∞ are plotted against the absolute values of the Fourier coefficients of the exact far field components u_j^∞ for $j = 1, 2, 3$ in Figure 6.3. For details on the numerical implementation of the Galerkin scheme we refer to [12].

Finally, to get an idea about the performance of the algorithm for noisy data, we redo this

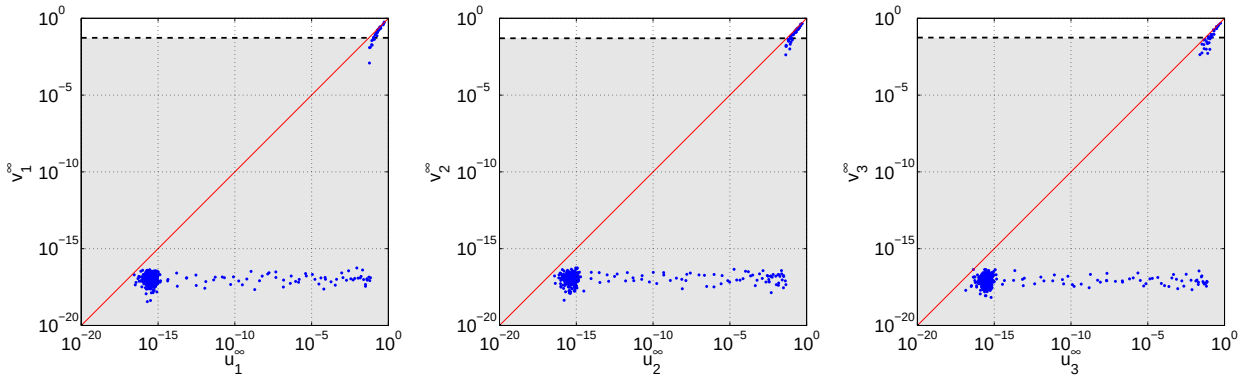

Figure 6.4: Same as Fig. 6.2, but using data containing 10% uniformly distributed noise ($\omega = 1/4$, $\alpha = 10^{-1}$, $\eta = 10^{-4}$, after 5 iterations in Algorithm 6.1 with 10^3 iterated soft thresholding steps each).

computation (without the post-processing step) but add 10% uniformly distributed relative error to the simulated far field data before splitting the far field pattern. We use the same a priori guess for the scatterers, and the same initial guess and parameters in Algorithm 6.1 as before, except for the regularization parameter in the soft thresholding procedure, for which we choose $\alpha = 10^{-1}$ to account for the noise in the data. The resulting scatter plots (after 5 iterations with 10^3 iterated soft thresholding steps each) are shown in Figure 6.4. The shaded region in these plots indicates the Fourier coefficients with absolute value less than 10% of their maximum. The results are clearly less accurate due to the noisy data, but the reconstructions of the largest Fourier coefficients are still useful. ◊

Conclusions

We have discussed a numerical scheme for the inverse problem of decomposing the far field pattern radiated by an ensemble of well separated compactly supported sources into the far field components radiated by each of these sources separately. We have developed an ℓ^1 characterization of these far field components and used it to reformulate the far field splitting problem as a constrained weighted ℓ^1 minimization problem. We have analyzed the well-posedness of this optimization problem, and verified the conditions for convergence of an iterated soft thresholding procedure to approximate the minimum numerically. We have also suggested an iterative reweighting strategy to successively improve the required a priori information on the approximate source locations, which in particular gradually enhances the stability of the splitting algorithm. Numerical examples for an inverse obstacle scattering problem confirm that this iteratively reweighted ℓ^1 far field splitting algorithm can handle much less accurate a priori information than the Galerkin far field splitting scheme considered in [12].

References

[1] M. Abramowitz and I. A. Stegun, *Handbook of mathematical functions, with formulas, graphs, and mathematical tables*, Dover Publications, New York, 1966.

[2] K. Bredies and D. Lorenz, Linear convergence of iterative soft-thresholding, *J. Fourier Anal. Appl.*, 14 (2008), 813–837.

[3] E. C. Candès, M. B. Wakin, and S. P. Boyd, Enhancing sparsity by reweighted ℓ_1 minimization, *J. Fourier Anal. Appl.*, 14 (2008), pp. 877–905.

[4] A. Chai, M. Moscoso, and G. Papanicolaou, Robust imaging of localized scatterers using the singular value decomposition and ℓ_1 minimization, *Inverse Problems*, 29 (2013), 025016.

[5] A. Chai, M. Moscoso, and G. Papanicolaou, Imaging strong localized scatterers with sparsity promoting optimization, *SIAM J. Imaging Sci.*, 7 (2014), pp.1358–1387.

[6] S. S. Chen, D. L. Donoho, and M. A. Saunders, Atomic decomposition by basis pursuit, *SIAM J. Sci. Comput.*, 20 (1999), pp. 33–61.

[7] D. Colton and R. Kress, *Inverse Acoustic and Electromagnetic Scattering Theory*, 2nd ed., Springer, Berlin, 1998.

[8] I. Daubechies, M. Defrise, and C. De Mol, An iterative thresholding algorithm for linear inverse problems with a sparsity constraint, *Comm. Pure Appl. Math.*, 57 (2004), pp. 1413–1457.

[9] A. J. Devaney, *Mathematical foundations of imaging, tomography and wavefield inversion*, Cambridge University Press, Cambridge, 2012.

[10] M. Grasmair, M. Haltmeier, and O. Scherzer, Sparse regularization with l^q penalty term, *Inverse Problems*, 24 (2008), 055020.

[11] M. Grasmair, M. Haltmeier, and O. Scherzer, Necessary and sufficient conditions for linear convergence of ℓ^1-regularization, *Comm. Pure Appl. Math.*, 64 (2011), 161–182.

[12] R. Griesmaier, M. Hanke, and J. Sylvester, Far field splitting for the Helmholtz equation, *SIAM J. Numer. Anal.*, 52 (2014), 343–362.

[13] R. Griesmaier, T. Raasch, and M. Hanke, Inverse source problems for the Helmholtz equation and the windowed Fourier transform, *SIAM J. Sci. Comput.*, 34 (2012), A1544–A1562.

[14] R. Griesmaier, T. Raasch, and M. Hanke, Inverse source problems for the Helmholtz equation and the windowed Fourier transform II, *SIAM J. Sci. Comput.*, 35 (2013), A2188–A2206.

[15] M. J. Grote, M. Kray, F. Nataf, and F. Assous, Wave splitting for time-dependent scattered field separation, *C. R. Math. Acad. Sci. Paris*, 353 (2015), 523–527.

[16] S. Kusiak and J. Sylvester, The convex back-scattering support, *SIAM J. Appl. Math.* 66 (2005), 591–615.

[17] M. Hanke, One shot inverse scattering via rational approximation, *SIAM J. Imaging Sci.*, 5 (2012), 465–482.

[18] F. Ben Hassen, J. Liu, and R. Potthast, On source analysis by wave splitting with applications in inverse scattering of multiple obstacles, *J. Comput. Math.*, 25 (2007), 266–281.

[19] R. Kress, On the numerical solution of a hypersingular integral equation in scattering theory, *J. Comput. Appl. Math.*, 61 (1995), 345–360.

[20] S. Kusiak and J. Sylvester, The scattering support, *Comm. Pure Appl. Math.*, 56 (2003), 1525–1548.

[21] S. Kusiak and J. Sylvester, The convex scattering support in a background medium, *SIAM J. Math Anal.*, 36 (2005), 1142–1158.

[22] S. Kusiak and J. Sylvester, The convex back-scattering support, *SIAM J. Appl. Math.* 66 (2005), 591–615.

[23] R. Potthast, F. M. Fazi, and P. A. Nelson Source splitting via the point source method, *Inverse Problems*, 26 (2010), 045002.

[24] R. Potthast, J. Sylvester, and S. Kusiak, A "range test" for determining scatterers with unknown physical properties, *Inverse Problems*, 19 (2003), 533–547.

[25] J. Sylvester, Notions of support for far fields, *Inverse Problems*, 22 (2006), 1273–1288.